Theses and Dissertations | 1. Thesis and Dissertation Collection, all items

1988-09

Natural convection liquid immersion cooling of a column of discrete heat sources in a vertical channel.

Knight, Daniel L.

http://hdl.handle.net/10945/23323

NAVAL POSTGRADUATE SCHOOL
Monterey, California

THESIS

K6161

Natural Convection Liquid Immersion Cooling
of a Column of Discrete Heat Sources
in a Vertical Channel

by

Daniel L. Knight
September 1988

Thesis Advisor: Yogendra Joshi

REPORT DOCUMENTATION PAGE

1a. REPORT SECURITY CLASSIFICATION UNCLASSIFIED		1b RESTRICTIVE MARKINGS			
2a SECURITY CLASSIFICATION AUTHORITY		3 DISTRIBUTION / AVAILABILITY OF REPORT Approved for public release; distribution is unlimited			
2b. DECLASSIFICATION / DOWNGRADING SCHEDULE					
4 PERFORMING ORGANIZATION REPORT NUMBER(S)		5 MONITORING ORGANIZATION REPORT NUMBER(S)			
6a NAME OF PERFORMING ORGANIZATION Naval Postgraduate School	6b OFFICE SYMBOL (If applicable) 69	7a NAME OF MONITORING ORGANIZATION			
6c. ADDRESS (City, State, and ZIP Code) Monterey, California 93943-5000		7b. ADDRESS (City, State, and ZIP Code) Monterey, California 93943-5000			
8a. NAME OF FUNDING / SPONSORING ORGANIZATION	8b. OFFICE SYMBOL (If applicable)	9. PROCUREMENT INSTRUMENT IDENTIFICATION NUMBER			
8c. ADDRESS (City, State, and ZIP Code)		10 SOURCE OF FUNDING NUMBERS			
		PROGRAM ELEMENT NO	PROJECT NO.	TASK NO	WORK UNIT ACCESSION NO

11. TITLE (Include Security Classification)
Natural Convection Liquid Immersion Cooling of a Column of Discrete Heat Sources in a Vertical Channel

12. PERSONAL AUTHOR(S)
KNIGHT, Daniel L.

13a. TYPE OF REPORT Master's Thesis	13b TIME COVERED FROM _____ TO _____	14. DATE OF REPORT (Year, Month, Day) 1988 September	15 PAGE COUNT 63

16 SUPPLEMENTARY NOTATION
The view expressed in this thesis are those of the author and do not reflect the official policy or position of the Department of Defense or the US Government

17	COSATI CODES		18 SUBJECT TERMS (Continue on reverse if necessary and identify by block number)
FIELD	GROUP	SUB-GROUP	Convective Flow, Thermal Transport, Flow Visualization

19 ABSTRACT (Continue on reverse if necessary and identify by block number)

Natural convection from a single column of eight in-line, rectangular, flush heat sources was examined. A vertical channel was formed by placing a movable shroud parallel to the test surface. The experimental program consisted of temperature measurements and flow visualizations. For a range of component power levels and channel spacings, surface temperatures of each heat source were measured at five locations using embedded thermocouple. The resulting steady state data was compared with corresponding measurements for an identical geometric arrangement of protruding heat sources. The flow visualization was carried out using a laser generated plane of light.

20 DISTRIBUTION / AVAILABILITY OF ABSTRACT ☒ UNCLASSIFIED/UNLIMITED ☐ SAME AS RPT ☐ DTIC USERS	21. ABSTRACT SECURITY CLASSIFICATION UNCLASSIFIED	
22a NAME OF RESPONSIBLE INDIVIDUAL Prof Joshi	22b TELEPHONE (Include Area Code) (408)646-3400	22c OFFICE SYMBOL 69Ji

DD FORM 1473, 84 MAR

83 APR edition may be used until exhausted
All other editions are obsolete

SECURITY CLASSIFICATION OF THIS PAGE

☆ U.S. Government Printing Office 1986—606-

UNCLASSIFIED

Natural Convection Liquid Immersion Cooling of a Column of Discrete Heat
Sources in a Vertical Channel

by

Daniel L. Knight
Lieutenant, United States Navy
B.S., The Citadel, 1979

Submitted in partial fulfillment of the
requirements for the degree of

MASTER OF SCIENCE
IN MECHANICAL ENGINEERING

from the

NAVAL POSTGRADUATE SCHOOL

ABSTRACT

Natural convection from a single column of eight in-line, rectangular, flush heat sources was examined. A vertical channel was formed by placing a movable shroud parallel to the test surface. The experimental program consisted of temperature measurements and flow visualizations. For a range of component power levels and channel spacings, surface temperatures of each heat source were measured at five locations using embedded thermocouples. The resulting steady state data was compared with corresponding measurements for an identical geometric arrangement of protruding heat sources. The flow visualization was carried out using a laser generated plane of light.

TABLE OF CONTENTS

LIST OF FIGURES

LIST OF SYMBOLS

Symbol	Description	Units
A	Area	m^2
A_s	Heater Surface Area	m^2
g	Acceleration due to Gravity	$\frac{m}{s^2}$
Gr^*	Flux-based Grashof Number	Dimensionless
h	Heat Transfer Coefficient	$\frac{W}{m^2 K}$
k_f	Fluid Thermal Conductivity	$\frac{W}{mK}$
k_{pg}	Plexiglass Thermal Conductivity	$\frac{W}{mK}$
L	Test Surface Length	m
$\bar{L}$	Characteristic Length	m
Nu	Nusselt Number	Dimensionless
Nu^*	Modified Nusselt Number	Dimensionless
NDT	Non-dimensional Temperature Excess	Dimensionless
P	Prandtl Number	Dimensionless
q''	Energy Flux Convected into the Fluid per Component	$\frac{W}{m^2}$
Q_{COND}	Energy Loss via Conduction Through the Test Surface	W
Q_{CONV}	Energy Convected into the Fluid per Component	W
Q_{in}	Energy into each Heater	W
S_n	Heater Element Number in Relation to the Leading Component	Dimensionless

T	Local Surface Temperature	$°C$
T_{amb}	Ambient Temperature	$°C$
T_{avg}	Average Component Temperature	$°C$
T_{film}	Film Temperature at which Fluid Properties are Evaluated	K
T_s	Surface Temperature	$°C$
v	Specific Volume	$\frac{m^3}{kg}$
x	Vertical Distance from Bottom Edge of Test Surface	m
z	Horizontal Distance from Component Center	m
β	Expansion Coefficient	$\frac{1}{K}$
μ	Dynamic Viscosity	$\frac{N_s}{m^2}$
ν	Kinematic Viscosity	$\frac{m^2}{s}$
θ	Temperature Difference Between Local Temperature and Ambient	K
θ_o	Temperature Scaling Factor	K

ACKNOWLEDGMENT

Natural convection from a single column of eight in-line, rectangular, flush heat sources was examined. A vertical channel was formed by placing a movable shroud parallel to the test surface. The experimental program consisted of temperature measurements and flow visualizations. For a range of component power levels and channel spacings, surface temperatures of each heat source were measured at five locations using embedded thermocouples. The resulting steady state data was compared with corresponding measurements for an identical geometric arrangement of protruding heat sources. The flow visualization was carried out using a laser generated plane of light.

I. INTRODUCTION

A. STATEMENT OF PROBLEM

With each successive increase in the scale of integration of micro-electronic circuits, there has been a need to improve cooling technologies. Currently, chip heat fluxes are approaching 50 W/cm^2, [Ref. 1]. Heat dissipation may be improved by using higher velocities of air, chilled water heat exchangers, or altering the system design to reduce its thermal resistance. These techniques are becoming less satisfactory and the limits of air and indirect liquid cooling have nearly been reached. If projected heat fluxes of 200 W/cm^2, [Ref. 1], are to be achieved, then direct liquid immersion becomes an attractive option, [Ref. 1, 6].

The performance and reliability of micro-electronic devices are very sensitive to junction temperatures. The failure rate of chips increase exponentially as the junction temperature increases. The long term reliability of circuit chips can be improved by 50% with every 10°C decrease in temperature that the device is maintained below its maximum operating temperature, [Ref. 2, 3, 4].

For a complete thermal analysis of any electronic package design, all three modes of heat transfer must be considered. Radiation effects are significant primarily in systems involving air cooling. Effects of conduction, however, must be evaluated in each cooling application. These may also be substantial during transients.

The convection heat transfer rate from a surface at temperature T_s with exposed surface area A to its surrounding fluid at temperature T_{amb} is given by Newton's Law of Cooling:

$$q = hA(T_s - T_{amb}) \qquad (1.1)$$

This is the definition of h, the convective heat transfer coefficient and not a phenomenological law.

Most available correlations for the convective heat transfer coefficient are usually valid for large heat sources. These are often good for determining the overall heat transfer from a single circuit board. Individual devices mounted on the substrate act as discrete heat sources and typically have higher average temperatures than those predicted by such text book correlations [Ref. 6].

Convection may be either forced or natural. Forced convection relies on a prime mover to displace the fluid and cause it to flow over the electronic package. This method of convection yields very high heat transfer coefficients and may become one of the primary means of cooling electronic packages as component heat fluxes continue to rise. Natural convection or buoyancy induced flow, results from body forces acting on density differences within the fluid. In many applications, these density gradients result due to the presence of temperature variations. The heat transfer coefficients are smaller than those associated with forced convection since the flow velocities are generally much smaller for natural convection. However, the resulting design of the package can be considerably simpler and more reliable than in other cooling arrangements.

B. OBJECTIVES

This experimental study was undertaken to determine the hydrodynamic and thermal characteristics of buoyancy induced flow resulting from several flush mounted

2

discrete heat sources on a vertical surface. The results from this study will be compared to those in Reference 7 where an array of rectangular protruding heat sources was used.

A single column of discrete heat sources was chosen since it provided a simple geometric arrangement simulating some of the modern electronic packages such as flat packs.

Specific objectives of this study were:

- To visualize the steady-state natural convection flow within a channel over a range of component power levels and channel widths.

- To measure component temperatures at each power level and channel width and develop heat transfer relationships for this geometry.

- To measure the temperature distribution within the fluid adjacent to the heated surface in the absence of a shrouding wall.

This study advances the work described in References 5 and 7 and is part of an ongoing effort to study natural convection liquid immersion cooling of electronic equipment.

II. EXPERIMENTAL

## A. GENERAL DESIGN CONSIDERATION

Equipment design and construction details are provided in Reference 5. Only system changes and a brief overview is presented here.

As seen in Figure 2.1, the test assembly consists of eight flush mounted foil heaters. Each heater (Figure 2.2) is a network of Inconel 600 conductor mounted on a Kapton backing. The heaters measured 23.9 mm in width by 7.8 mm in height. They formed a single column on a plexiglass substrate. The substrate measured 25.4 mm square and was 12.7 mm thick. The column of heaters was centered on the substrate and each heater was spaced 25.4 mm center to center from an adjacent heater. Another piece of plexiglass identical to the substrate without the heaters was used as an adjustable shroud wall to form the channel. This shroud was used to simulate the back side of a neighboring circuit board.

Five copper-constantan thermocouples of 0.127 mm diameter wire were used for temperature measurements on each heater. The thermocouples were embedded within 6 mm deep slots in the substrate. For each heater, one thermocouple bead was located at the foil center and the remaining four were at the centers of each edge of the heater. All wires were routed along 6 mm deep grooves cut below the heater placement slots. All wiring came out through the back of the test surface through drilled holes in the substrate. After all heaters and wires were in place, these holes were sealed with a low conductivity adhesive. Omega Bond 101, a high conductivity adhesive, was used to bond the thermocouples in place and to electrically insulate the thermocouple beads from the heater foils. A sixth thermocouple for each heater

4
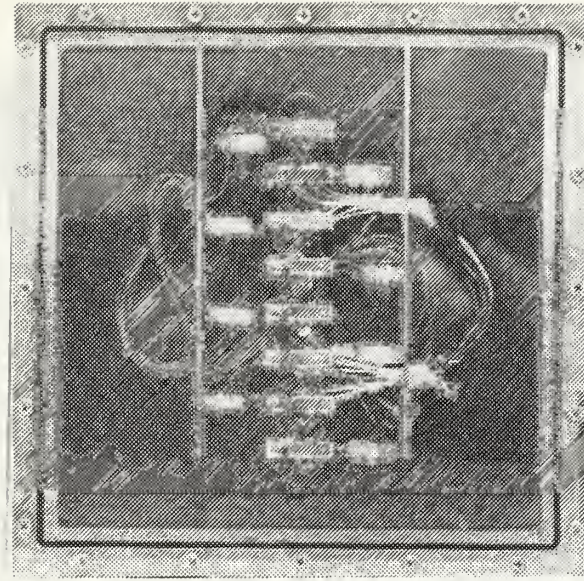
Figure 2.1: Assembled Test Surface

was centered behind the heater on the back side of the plexiglass substrate. This was used to estimate conduction losses through the substrate.

A 0.127 mm diameter, copper-constantan thermocouple probe (Figure 2.3) was constructed. This probe was attached to a three dimensional traverse and used to measure the temperature distribution within the fluid adjacent to the test surface. The foil heaters were powered using a regulated D.C. power supply as described in Reference 5.

The test surface was immersed in an open, one cubic meter tank constructed from plate glass and insulated on all sides. For flow visualization, particles of pliolite were suspended in the de-ionized water. Pliolite is an inert substance with a specific gravity of 0.93. These particles were illuminated by aiming an eight milliwatt helium neon laser through a cylindrical lens to split the light beam into a plane of light.
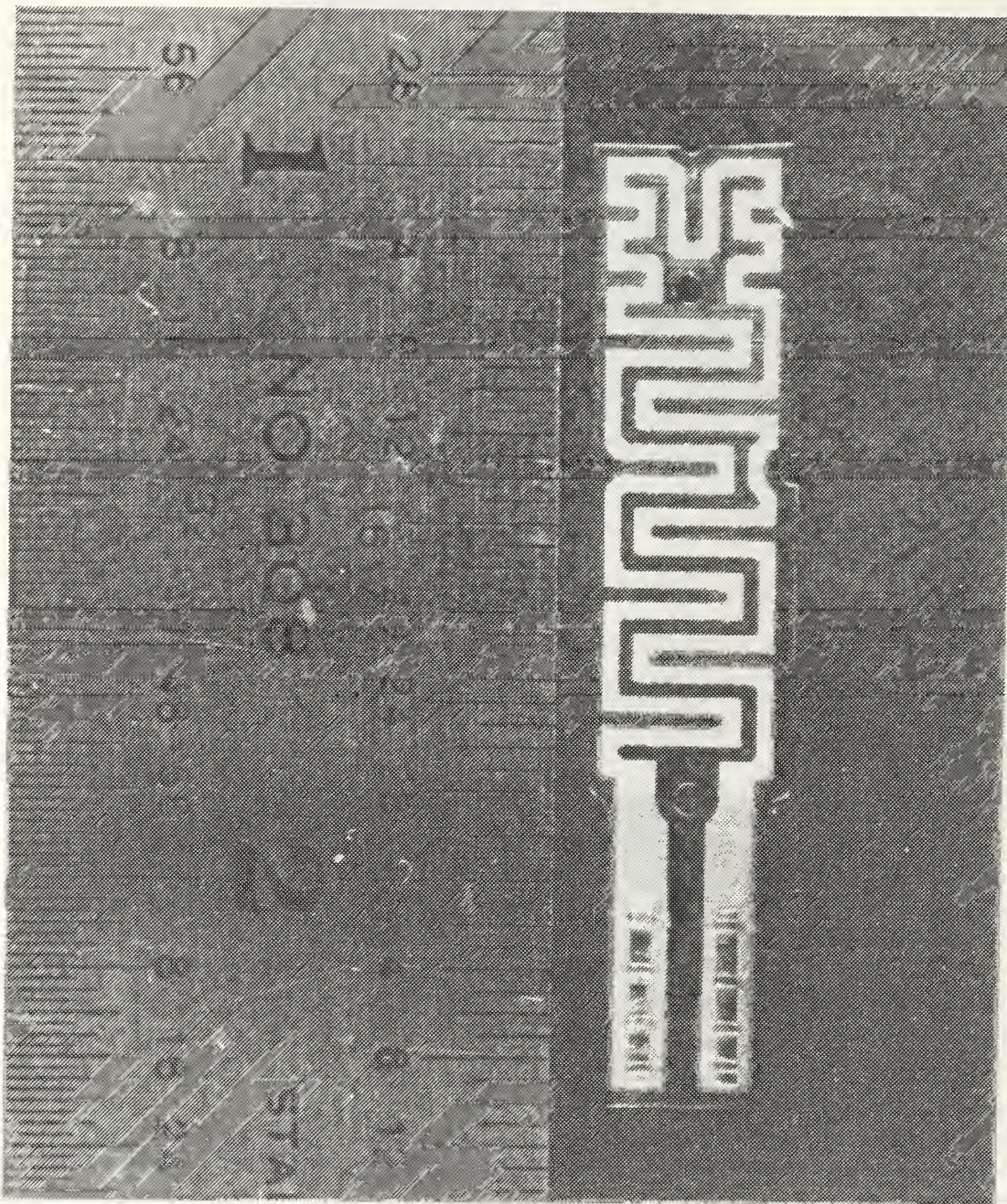
Figure 2.2: Foil Heater

6
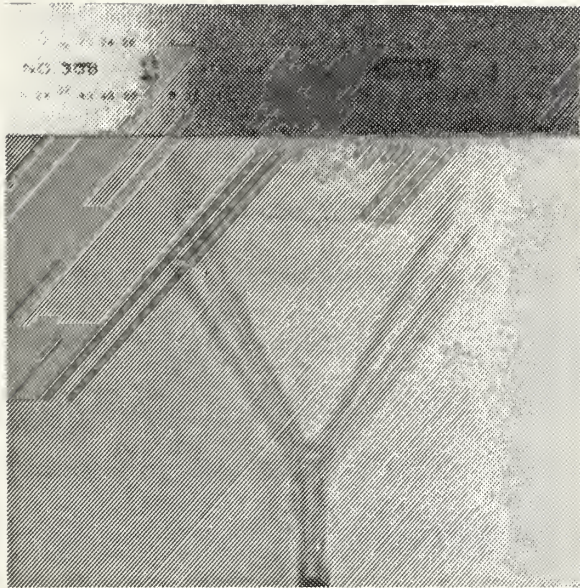
Figure 2.3: Traversing Thermocouple Probe

By using a motor driven camera and an intervalometer, extended time exposure photographs of the flow patterns within the illuminated plane were obtained.

B.   EXPERIMENTAL PROCEDURE

Details of data acquisition techniques are provided in Reference 5, hereafter referred to as the initial study. The follow-on study by Willson [Reference 7] will be referred to as the previous study.

Power settings of 0.2, 0.5, 1.0, 1.2, 1.5, and 2.0 watts were used for each channel width. The shroud was adjusted for channel spacings of 1.5 mm, 3.0 mm, 5.0 mm, 9.0 mm, 12.0 mm and 15.0 mm. With the shroud removed, an infinite channel spacing was created.

When measuring the steady state temperatures of each heater element, measurements were taken at 10 minute intervals and compared with the previous data

run. When all thermocouple measurements varied less than $0.05°C$, the final steady state temperature measurements were recorded. The termperature acquisition program of the previous study [Appendix A] was executed to record and store data.

Ambient temperature was the average temperature from three thermocouples located in the fluid near the top, bottom and center of the tank. All experiments were stopped if these three temperatures varied by more than $0.1°C$.

When measuring the fluid temperature with the movable probe, the data acquisition computer was programmed to continuously monitor the voltage output from the traversing thermocouple probe. This allowed for point to point temperature measurements within the flow.

After all data was recorded, the substrate was painted black to minimize light reflection. Particles of pliolite were mixed with the distilled water to visualize fluid flow. The f stop of the camera was set to 2.8 and exposure time for all photographs was 20 seconds. The camera was mounted on a tripod, approximately three inches from the glassplate wall of the tank. Camera height was adjusted and the laser was aligned so that all eight heater surfaces would be in the field of view. When the shroud was in position, the camera angle was inclined slightly to avoid the undesirable light reflection off the shroud. A shroud spacing of 12 mm from the substrate was the minimum channel width at which useful pictures could be taken. Figure 2.4 shows the arrangement of the camera, laser and test surface.

C. DATA ANALYSIS

The convected rate of energy from each heater was determined using an energy balance where:
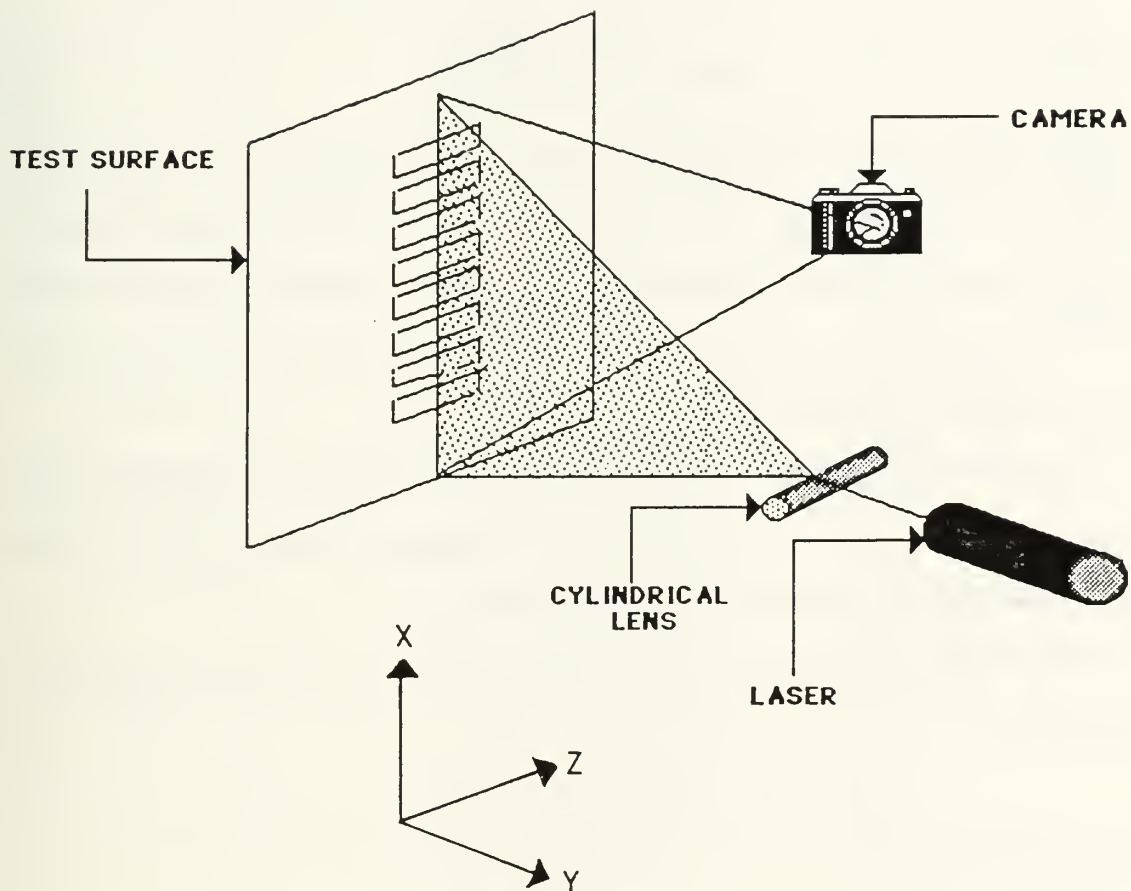
$$Q_{CONV} = Q_{in} - Q_{COND} \qquad (2.1)$$

Figure 2.4: Laser and Camera Arrangement for Photography in the x-y Plane.

9

The energy in Q_{in} was regulated by the power supply and determined as described in the initial study. The energy loss by conduction was estimated by using Fourier's law of conduction for one dimension:

$$Q_{COND} = A_s k_{pg} \frac{\Delta T_{avg}}{\Delta x} \tag{2.2}$$

A_s is the surface area of each heater element, k_{pg} is the thermal conductivity for plexiglass. ΔT_{avg} is the temperature difference between the temperature average of the five thermocouple locations on the heater and the temperature at the back side of the substrate. Δx represents the minimum thickness of the substrate accounting for the grooves cut for wire routing.

A characteristic length, $\bar{L}$, based on the geometric dimensions of the heaters was chosen for determining non-dimensional temperature excess, $\frac{\theta}{\theta_o}$, a flux based Grashof number, Gr^*, and Nusselt number, Nu.

The characteristic length is the heater surface area divided by the heater perimeter.

$$\bar{L} = \frac{A_s}{p} \tag{2.3}$$

Local heat transfer relationships were determined by the following equations:

$$q'' = \frac{Q_{CONV}}{A_s} \tag{2.4}$$

$$\theta_o = \frac{q'' \bar{L}}{k_f} \tag{2.5}$$

$$h = \frac{q''}{\Delta T} \tag{2.6}$$

10

$$Gr^* = \frac{g\beta q'' \bar{L}^4}{k_f \nu^2} \tag{2.7}$$

$$Nu = \frac{h\bar{L}}{k_f} \tag{2.8}$$

$$\theta = \Delta T \tag{2.9}$$

$$NDT = \frac{\theta}{\theta_o} \tag{2.10}$$

The data reduction program [Appendix A] was used for all calculations. Sample calculations are contained in Appendix B. The various symbols used above are defined in the List of Symbols.

Fluid properties were determined from curve fits listed by Willson [Reference 7]. These are based on the data provided in Incropera and Dewitt [Reference 8]. All properties were evaluated at a film temperature. The film temperature was determined for each case from the local and ambient temperatures.

A non-dimensional length, $\frac{X}{L}$, was used in the presentation of the data. The vertical length $\frac{X}{L}$ is the distance from the bottom edge of the substrate to the local point of interest divided by the overall length of the substrate.

Quantitive developments were expressed as plots of:

- Nu vs. Gr^*

- Non-dimensional local temperature excess vs. local thermocouple location.

- Temperature distribution in the fluid adjacent to the test surface.

III. TRANSPORT ADJACENT TO AN ISOLATED VERTICAL SURFACE

A. FLOW VISUALIZATION

Photographs of the steady state natural convection flow in the x-y plane are shown in Figure 3.1. The laser was aligned so that the plane of light would pass through the geometric center of the heated region of each component. This figure presents all elements at input power levels of 0.2, 1.0 and 2.0 watts respectively from left to right.

Buoyancy forces near the heaters create a strong upward flow. The flow appears to be laminar and is parallel to the substrate after the first component. A boundary layer begins to develop out from the leading heater. The boundary layer thickness increases to about 2.5 component heights at the trailing element. At 1.0 watt, the boundary layer is about 2.0 component heights thick and decreases to about 1.0 component height in thickness at the trailing element for 2.0 watts. The fluid velocity increases and the thickness of the boundary layer decreases with increasing component power input. Ambient fluid is entrained below and along the length of the boundary layer. Figure 3.2 visualizes the flow in the x-z plane at the respective power levels of the previous figure. The flow is vertical along the array for about the width of the heated region of the strips. Weak entrainment from the sides is evident. Side entrainment increases with increasing component heat input. Figure 3.2 clearly shows that for the region along the array, the flow can be treated to an excellent approximation as two dimensional.
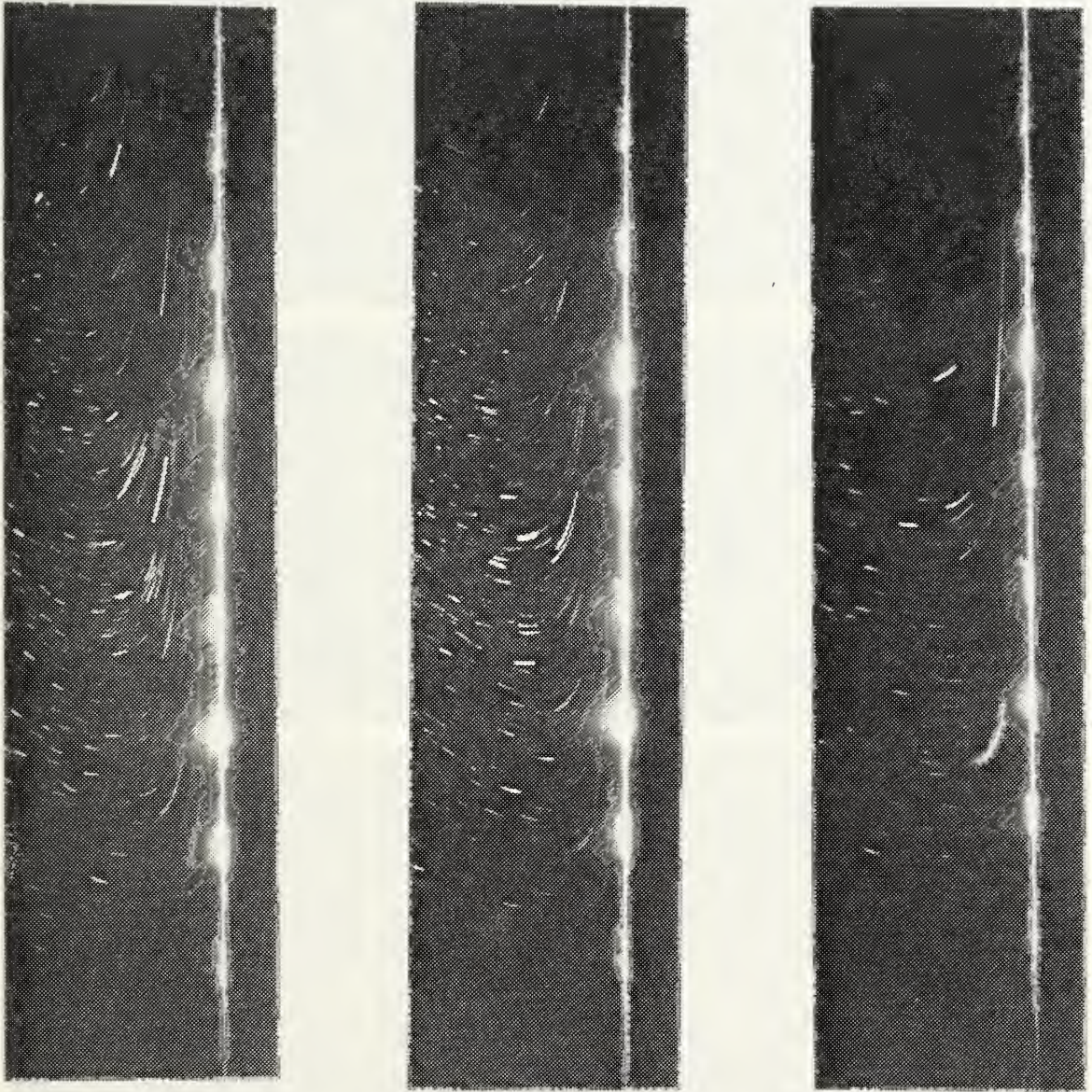
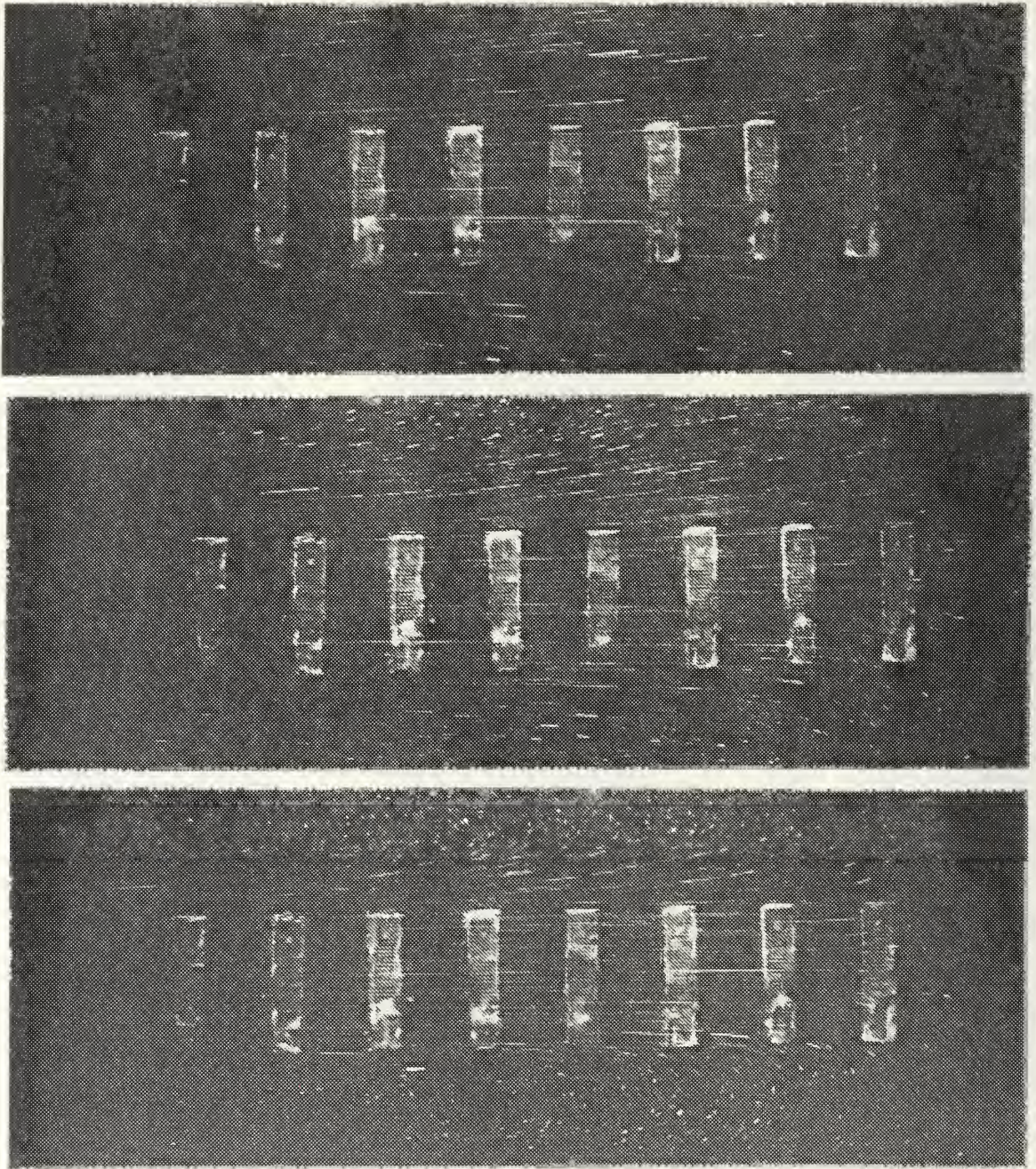Figure 3.1: Steady Flow in the x-y Plane for Power Levels of 0.2, 1.0 and 2.0 Watts

Figure 3.2: Flow in the x-z Plane at 0.2, 1.0 and 2.0 Watts

14

B. QUANTITATIVE

Figure 3.3 is a non-dimensional representation of local temperature excess levels measured at all thermocouple locations for an input power level of 2.0 watts. As expected, the measured component center temperatures were the highest. The top edge temperatures always exceeded the temperatures at the other edges. The left and right edge temperatures differed by a maximum of 22% at 2.0 watts. The heater strip had an 11 mm tab on the left side for power lead connections. Left edge conduction losses were therefore expected to be greater than the right side, resulting in slightly lower temperatures on the left. After the third component, the bottom edge temperatures exceeded the excess temperature of the sides. The side edges benefited more from fluid entrainment than the bottoms which are in the wake of the heated upstream components. In all experiments, the right edge temperature for component seven was lower than the established trend. It is believed that the thermocouple placement at this location may have slipped when the heater foil was pressed into place.

Heat transfer coefficients were computed from the data as outlined in equation 2.6. They indicated a downstream decreasing trend at a given power level. This is expected since the non-dimensional temperature excess is inversely proportional to h. As seen in Figure 3.3, the general trend tends to be increasing downstream excess temperatures.

As the component heat flux is increased, the buoyant flow becomes more vigorous. The component temperature levels, as a result, decrease. The calculated heat transfer coefficients are greater than those for the same component at lower power levels. With the larger values of h at higher power levels, there is a corresponding decrease in the non-dimensional temperature excess.
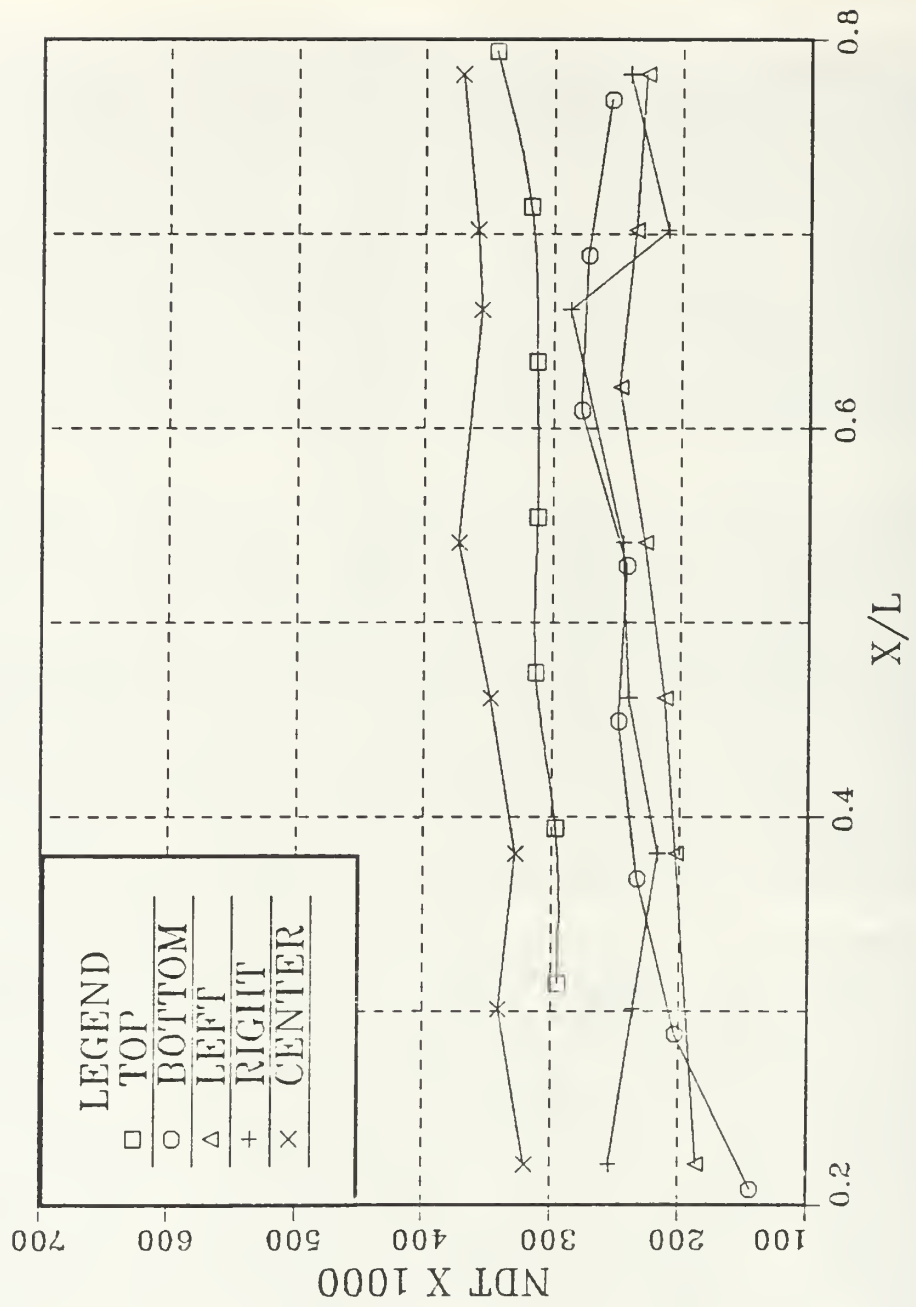
Figure 3.3: Non-dimensional Temperature Excess vs. Position: 2.0 Watts

16

Figure 3.4 is a logarithmic scatter plot of Nu vs. Gr^*. The cluster of data points at approximately a single Gr^* represents the Nusselt numbers for component centers at each power level. The Nusselt numbers decrease for downstream components, due to the increasing component temperatures.

As in the previous study, a modified Nusselt number, Nu^*, was calculated by using a scaling factor to account for the increase in convected energy of the flow at downstream locations.

$$Nu^* = Nu_n \times S_n^{\frac{1}{14}} \qquad (3.1)$$

Nu_n and S_n are the local Nusselt numbers with the respective heater element numbers.

This modified data is plotted in Figure 3.5. The linear least squares fit through the data with a $\pm 5\%$ band is also presented. Using the scaling factor above, nearly all of the modified data falls within this band. Based on this curve fit, the following heat transfer relationship for the given array geometry was obtained:

$$Nu^* = 1.115(Gr^*)^{.12} \qquad (3.2)$$

for $250 < Gr^* < 7000$ and $Pr \sim 7$.

C. EFFECT OF COMPONENT SPACING ON HEAT TRANSFER

Now that a heat transfer correlation has been developed for the given geometry of the array, it is desired to see how a change in component spacing would affect these relationships. This was achieved by powering every other and every third heater. This had the same effect as heater elements spaced 50.8 mm and 76.2 mm center to center. The resulting variations of non-dimensional temperature excess at the heater centers are shown in Figures 3.6 and 3.7.
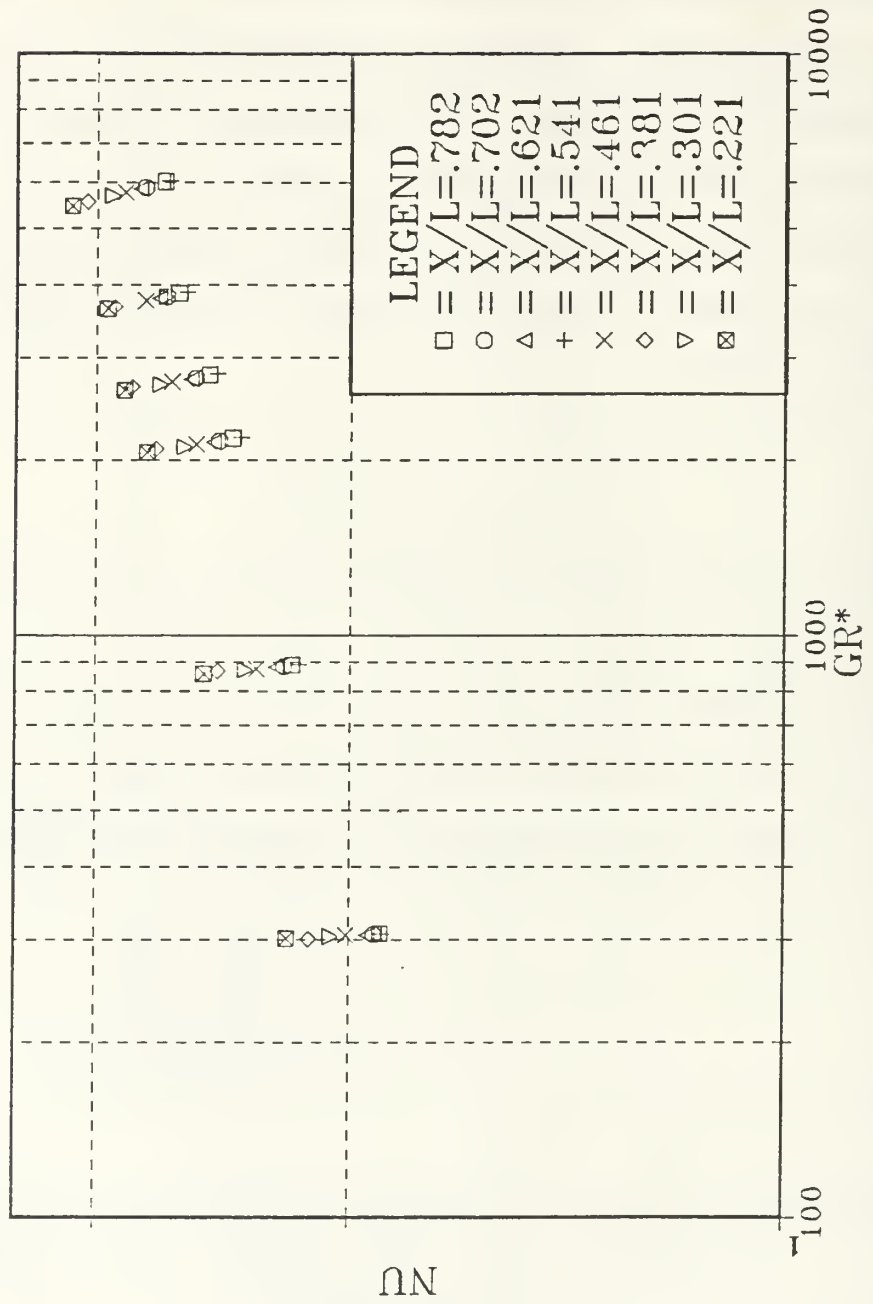
17

Figure 3.4: Data for Nusselt Number vs. Flux-Based Grashof Number
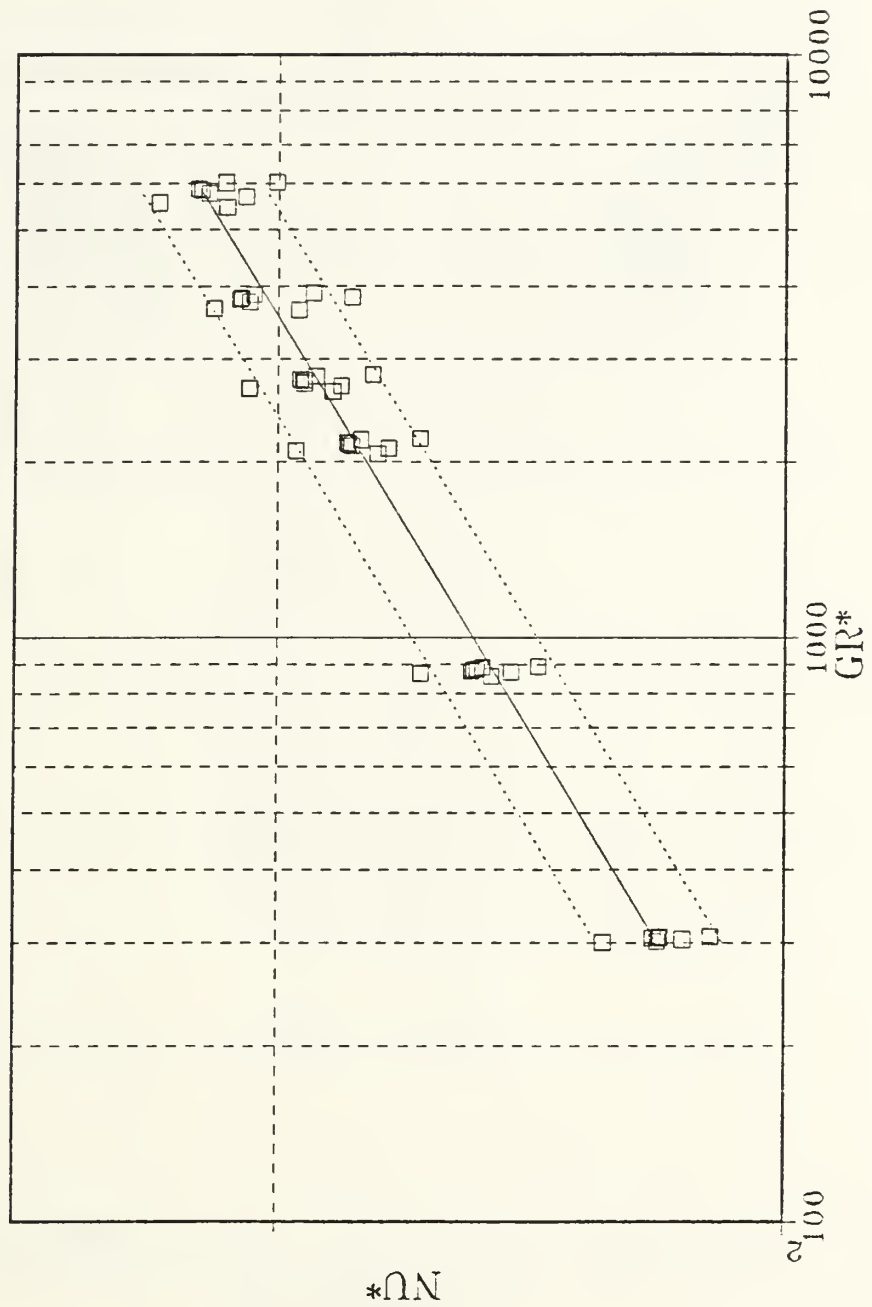
Figure 3.5: Modified Nusselt Number vs. Flux-Based Grashof Number with Least Squares Fit
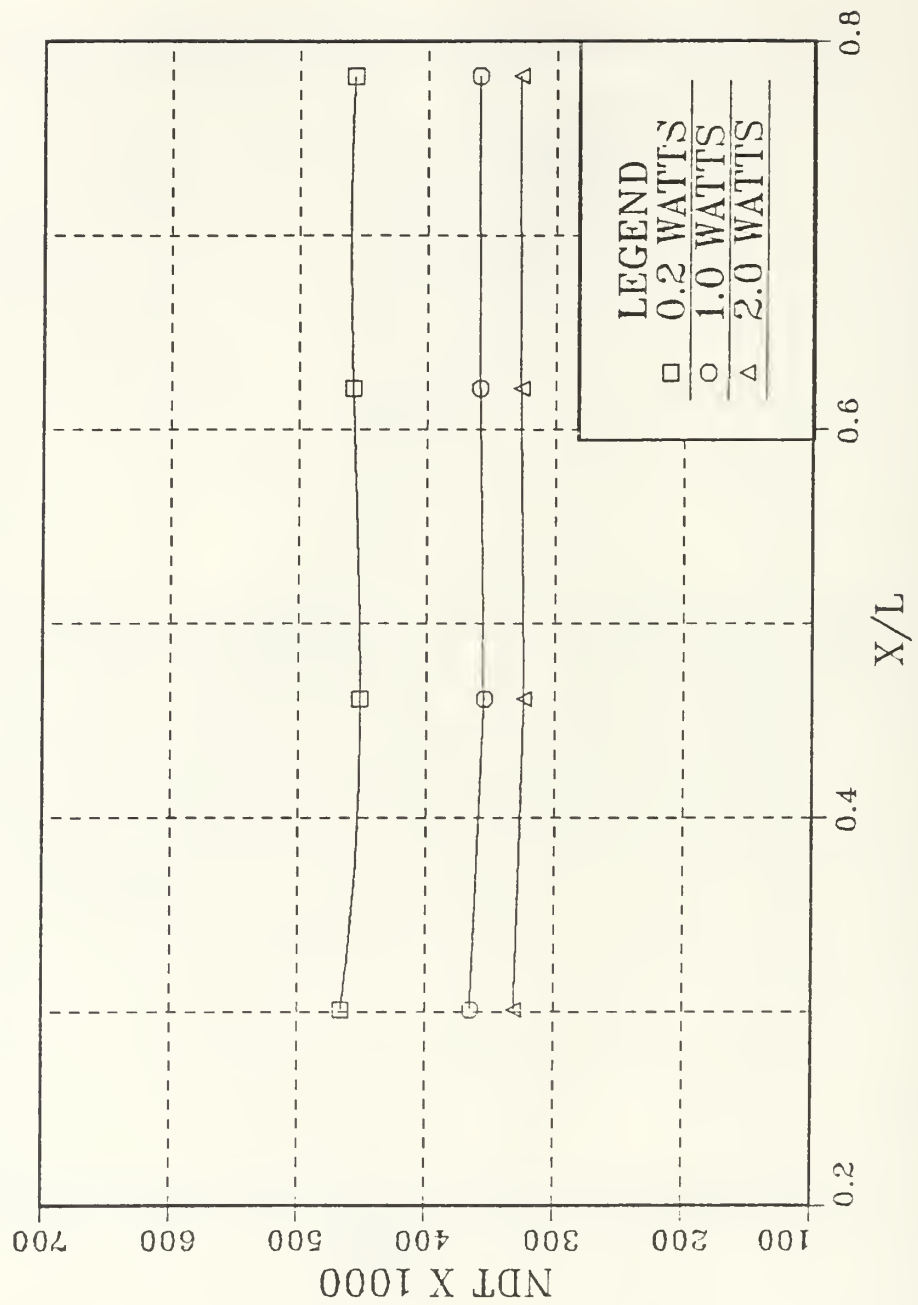
19

Figure 3.6: Non-dimensional Temperature Excess vs. Position with Four Elements Powered
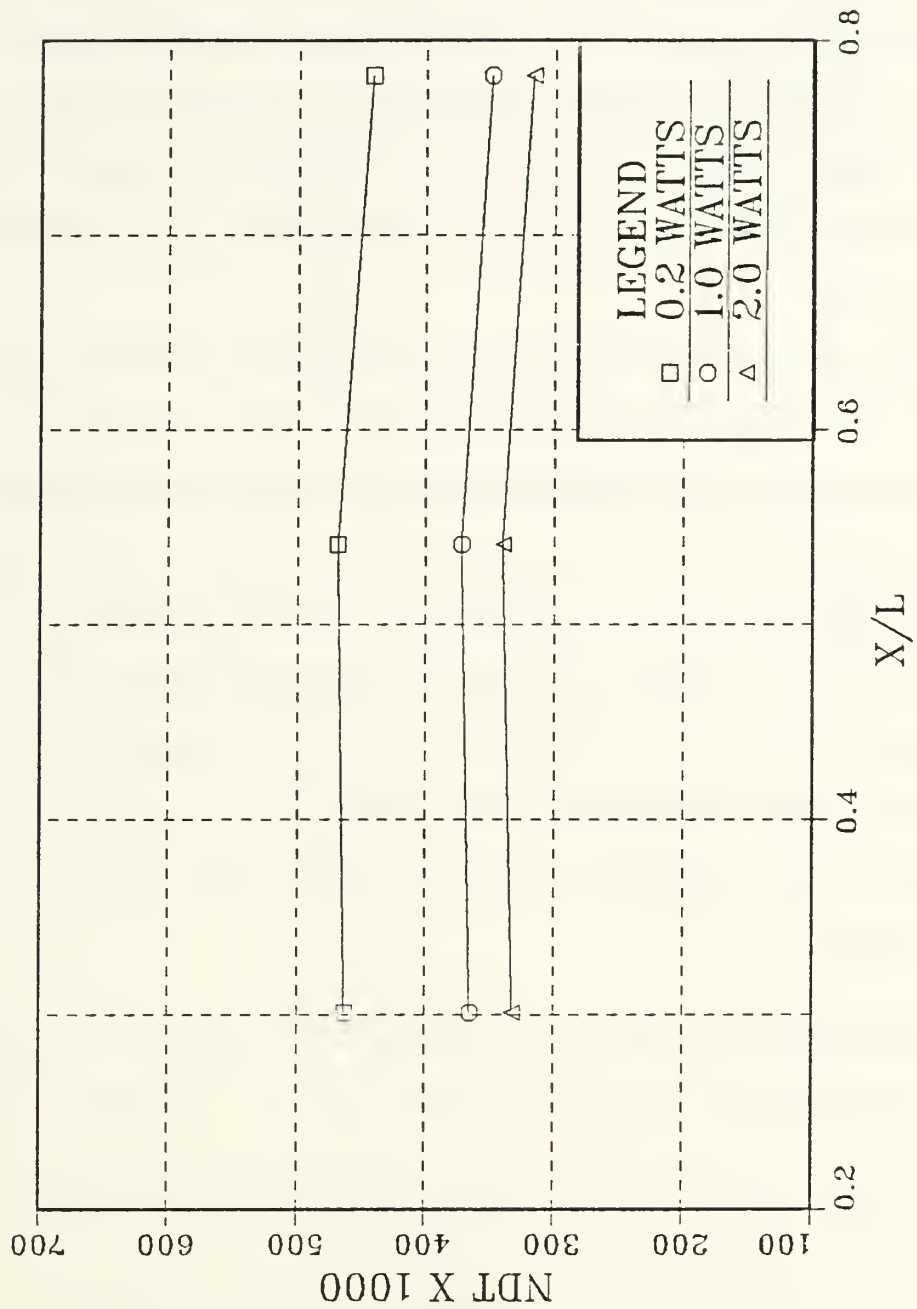
Figure 3.7: Non-dimensional Temperature Excess vs. Position with Three Elements Powered

21

When heaters 2, 4, 6 and 8 are powered, there is a slight decrease in the non-dimensional temperature at the first downstream component beyond the leading heater. Further up, component temperatures vary little from that of the second heater. When heaters 2, 5, and 8 are powered, the first two component temperatures remain unchanged. The trailing heater has a small drop in its non-dimensional temperature.

For the increased component spacings in Figures 3.6 and 3.7, the convected energy due to upstream heaters has only a weak effect on downstream components. The fluid momentum resulting from the buoyancy forces actually provides moderate improvement in heat transfer for the downstream heaters. Heat transfer relationships were obtained for all components by treating the elements in the array as single heaters. The resulting component based Nusselt numbers became almost independent of the downstream component position in the expanded array. These are plotted against the flux-based Grashof number in Figures 3.8 and 3.9. The least square fit to the correlated data for all unshrouded heaters is shown for comparison in each figure.

D. TEMPERATURE MEASUREMENTS WITHIN THE FLUID

Measurements of the thermal transport in the fluid adjacent to the test surface were made using the movable thermocouple probe. The thermocouple junction was initially centered on each component and then moved outward in the direction normal to the substrate. Temperatures are seen in Figure 3.10 for input power levels of 0.2 and 1.0 watts. The thermal boundary layer in both cases is well within the momentum exchange region which is approximately 1.6 cm thick for component 8 at 1.0 watt. This is expected due to the relatively large Pr of about 7.0 for water.
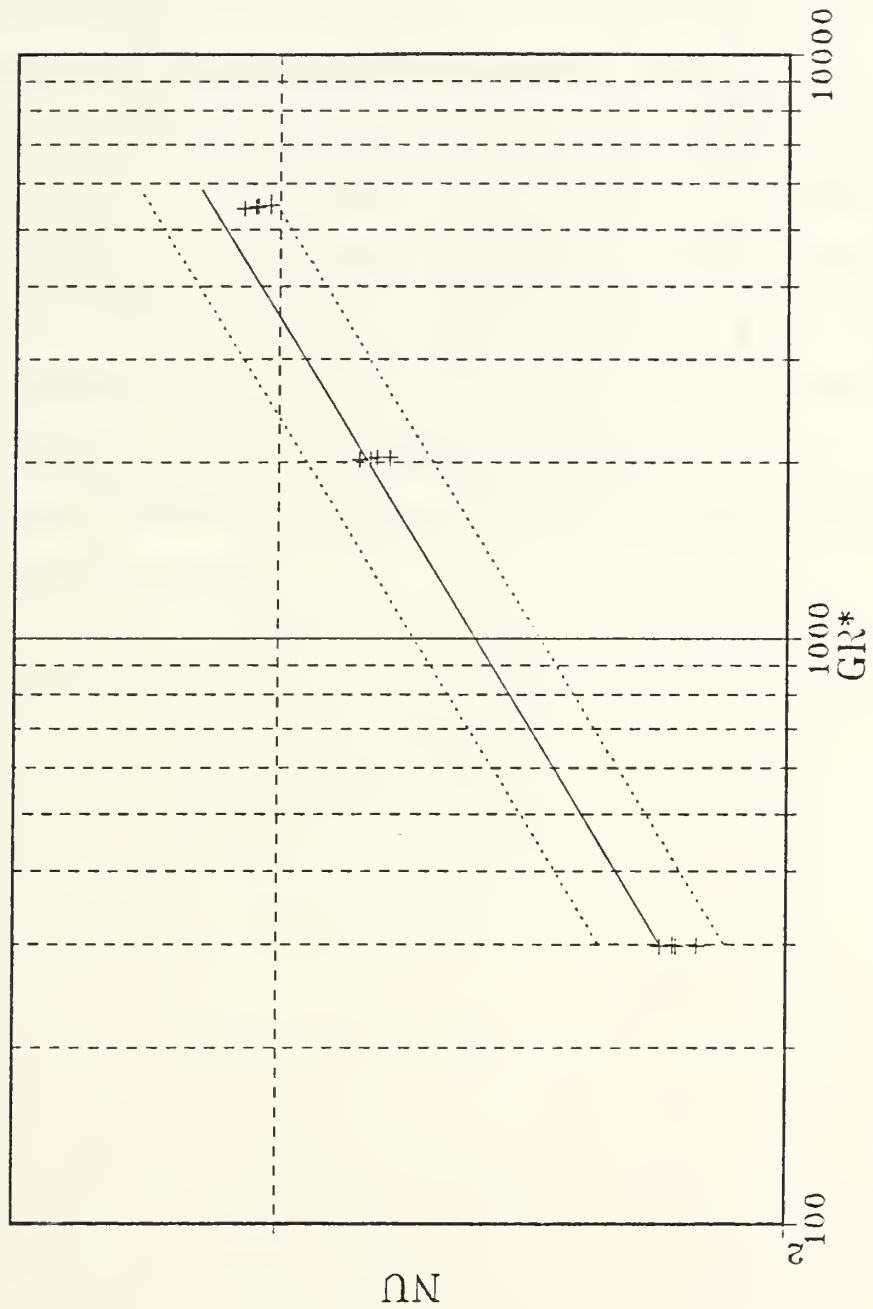
Figure 3.8: Nusselt Number vs. Flux-based Grashof Number with Four Elements Powered
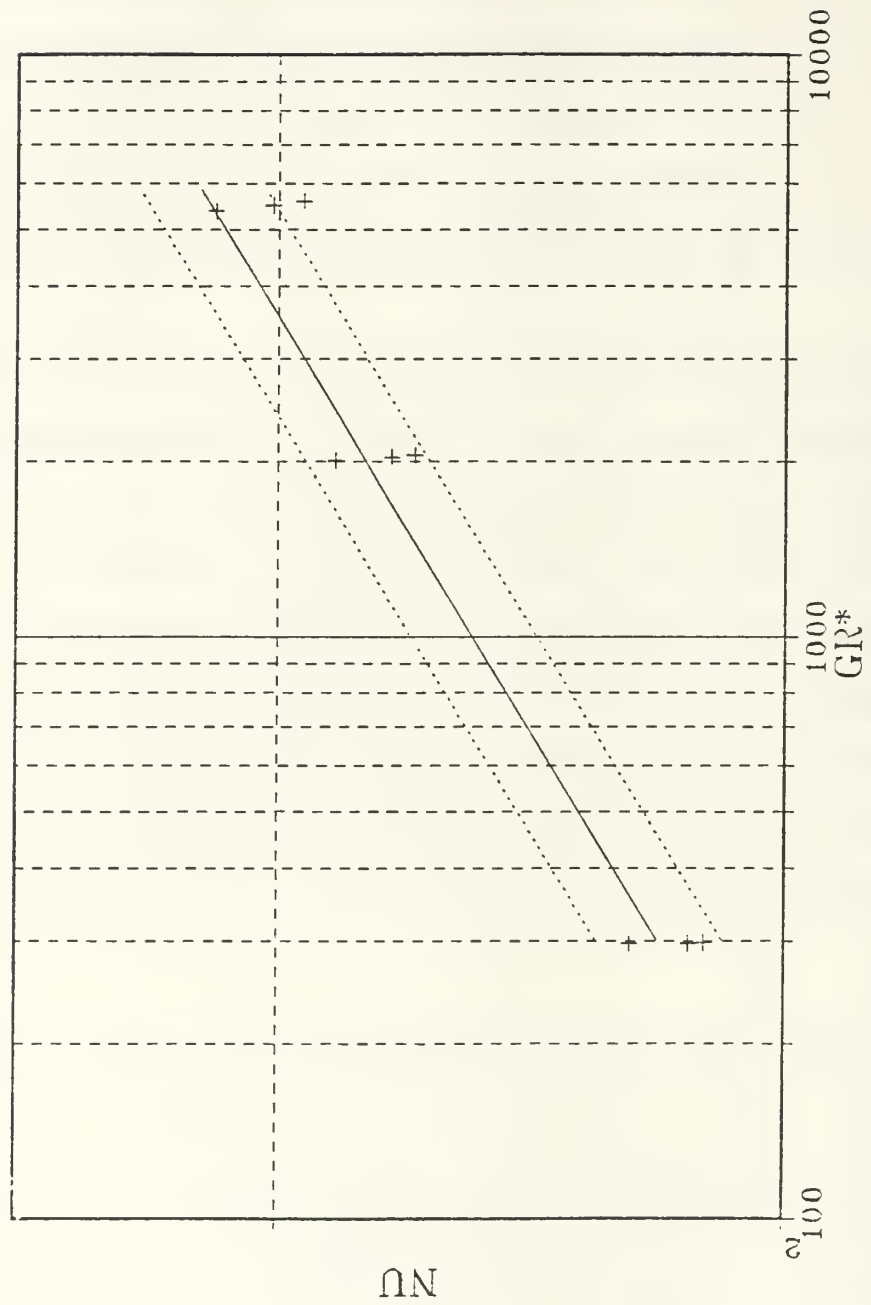
Figure 3.9: Nusselt Number vs. Flux-based Grashof Number with Three
Elements Powered

24

Figure 3.10 suggests that it may be possible to move a shroud wall to within one component height without changing the rate of heat transfer significantly.

The traversing probe was slowly swept spanwise in the z-direction past the centers of the heaters 3, 5 and 8 at a distance of 1.0 mm outward in the y-direction from the heater surface. Resulting temperature variations are shown in Figure 3.11 for a power level of 1.0 watt. The component center is referred to as 0.0. A scale line provides a reference for the width of the heated region of each component. A large drop in temperature is seen to occur beyond $Z = \pm 6$ mm. For the center 50% of each heater, there is relatively small change in temperature, again suggesting a largely two dimensional flow there.

Figure 3.10: Fluid Temperature Distribution in the y-Direction for 0.2 and 1.0 Watts

26

Figure 3.11: Spanwise Fluid Temperature Distribution

27

IV. TRANSPORT IN A VERTICAL CHANNEL

A plexiglass shroud, simulating the back side of a neighboring circuit board, was positioned to form a vertical channel of various widths.

A. FLOW VISUALIZATION

Useful photographs could only be taken with the shroud positioned no closer than 12 mm from the substrate. All visualizations presented are at power levels of 0.2, 1.0 and 2.0 watts respectively. Figure 4.1 shows the natural convection fl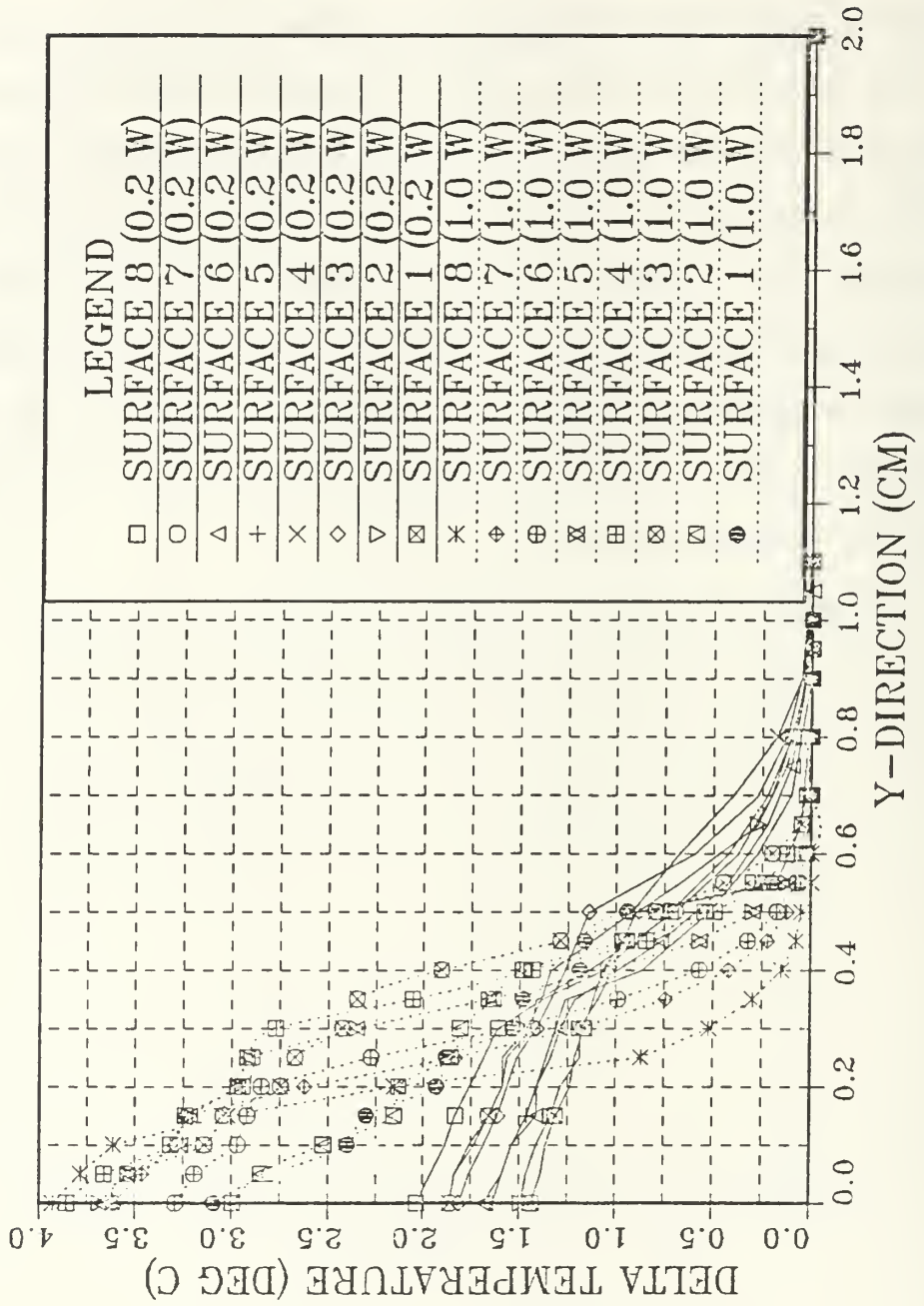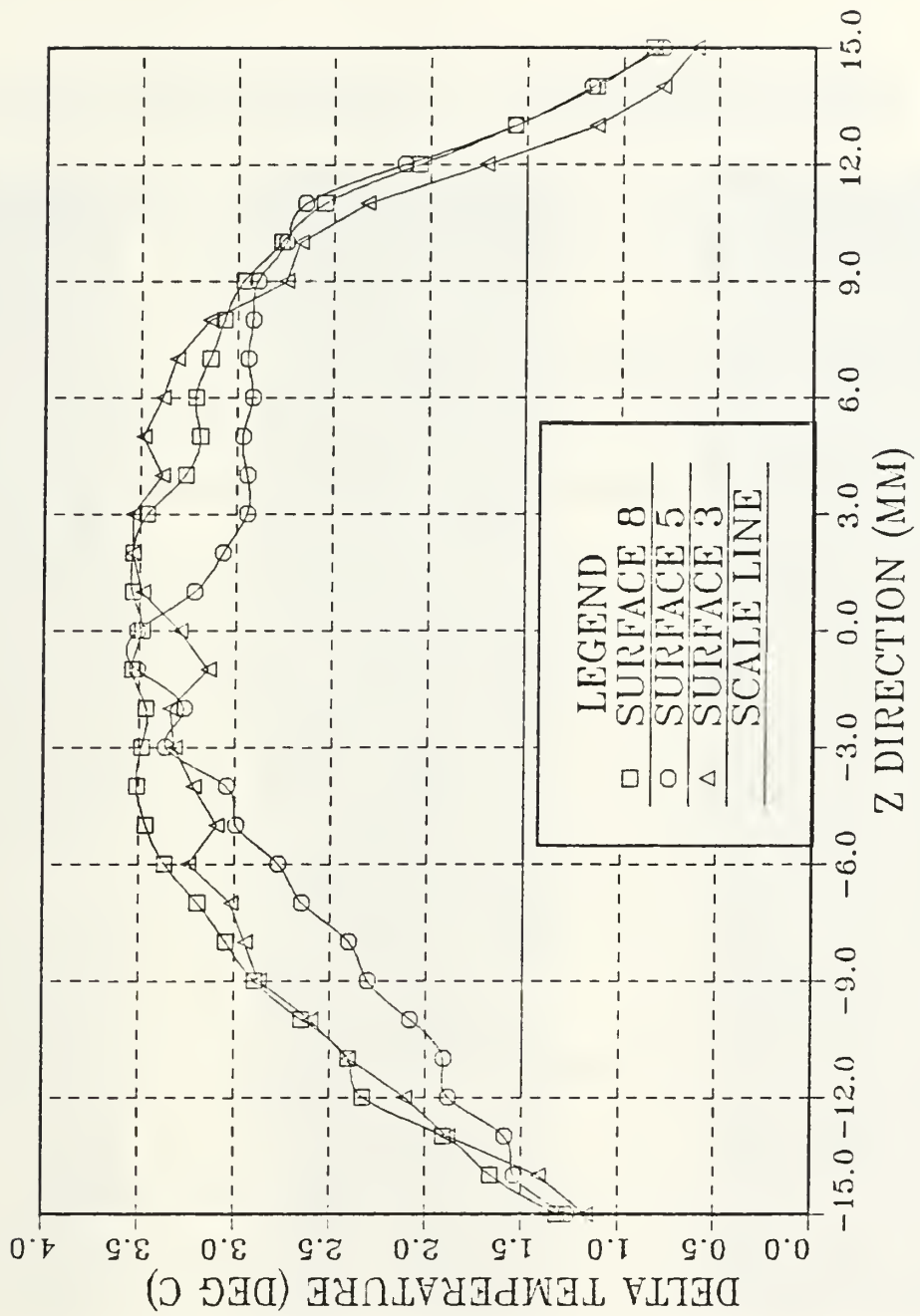ow in the x-y plane with the shroud positioned 12 mm from the substrate. The shroud only allows entrainment from the sides and bottom. Initially the flow is not parallel to the channel walls. The entrained fluid entering from the bottom has velocity components in the x and y directions. As the boundary layer develops to the width of the channel, the flow is straightened and conforms to the channel. This same flow behavior occurs when the channel width is increased to 15 mm as shown in Figure 4.2 The effects of entrainment are more noticeable downstream since the boundary layer has more time to develop with the wider channel.

Figure 4.3 presents flow visualization in the x-y plane with the shroud positioned 6 mm from the substrate. These photographs were taken with the camera aligned in the direction normal to the surface. With the shroud in position, side entrainment is much more pronounced than the case without a shroud [Figure 3.2].

B. QUANTITATIVE

Figures 4.4 and 4.5 are non-dimensional representations of temperature excess levels for all center located thermocouples for each shroud condition. These two
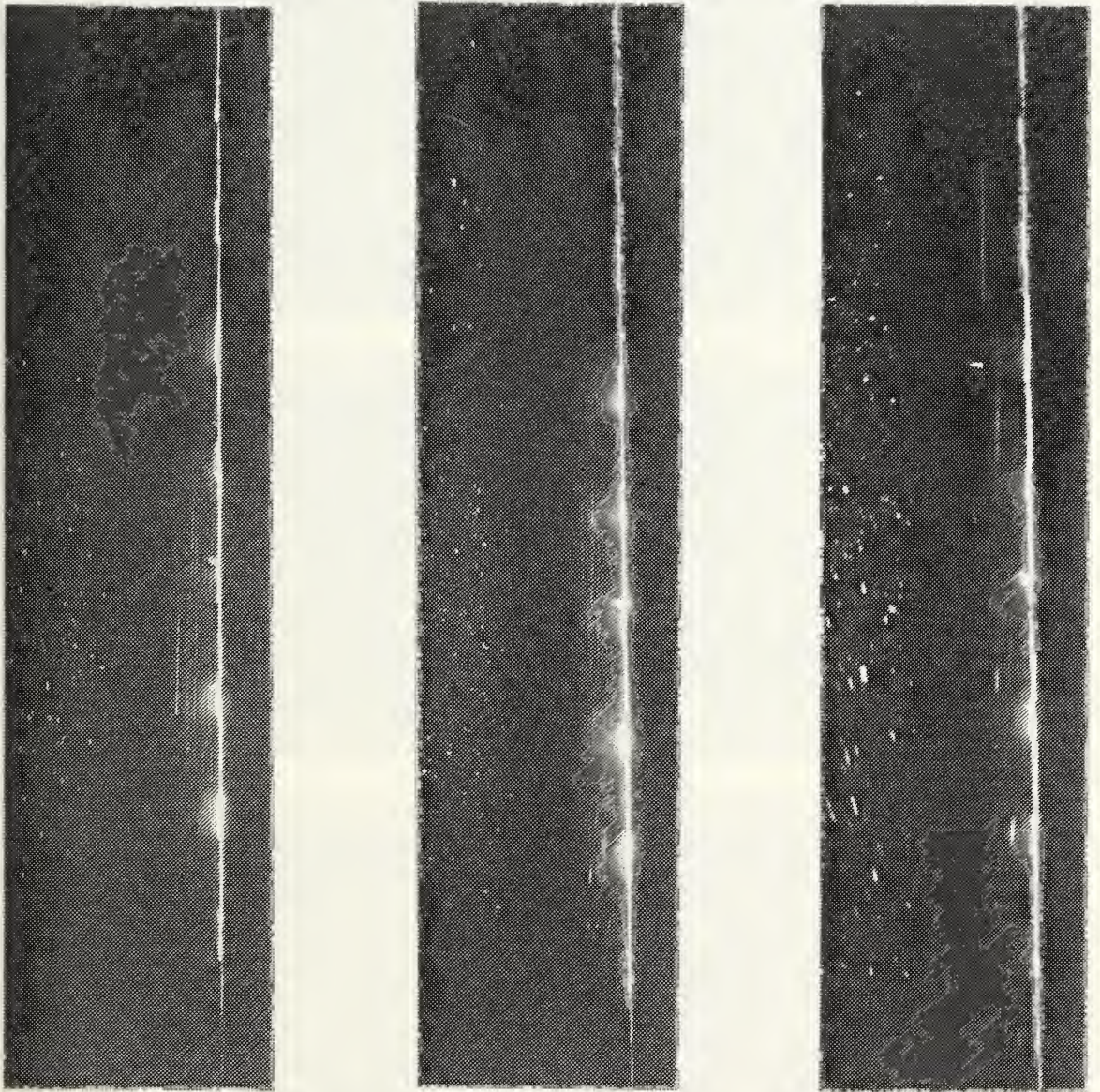
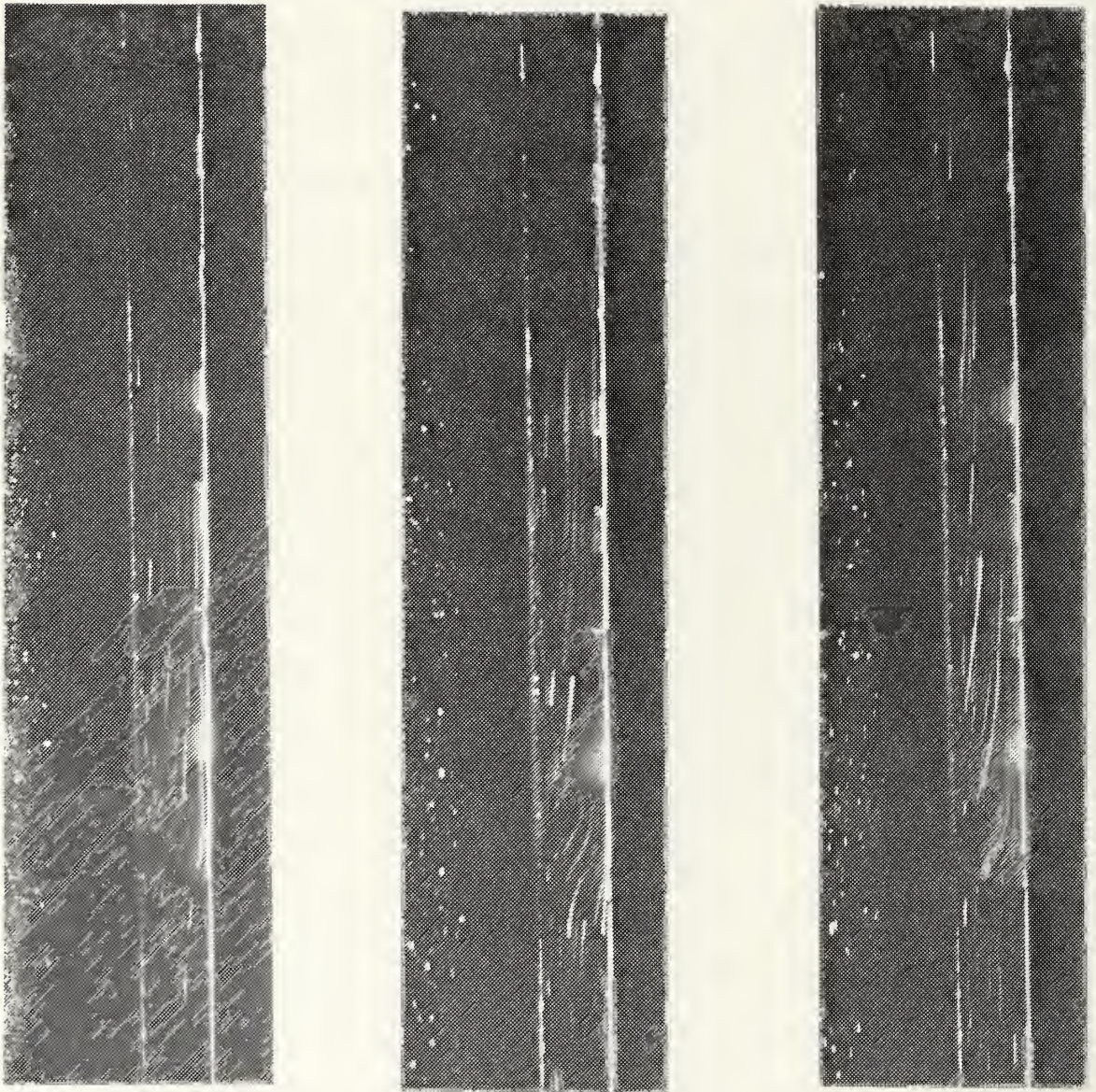Figure 4.1: Steady Flow in the x-y Plane for Power Levels of 0.2, 1.0 and 2.0 Watts with 12 mm Shroud

Figure 4.2: Steady Flow in the x-y Plane for Power Levels of 0.2, 1.0, 2.0 Watts with 15 mm Shroud
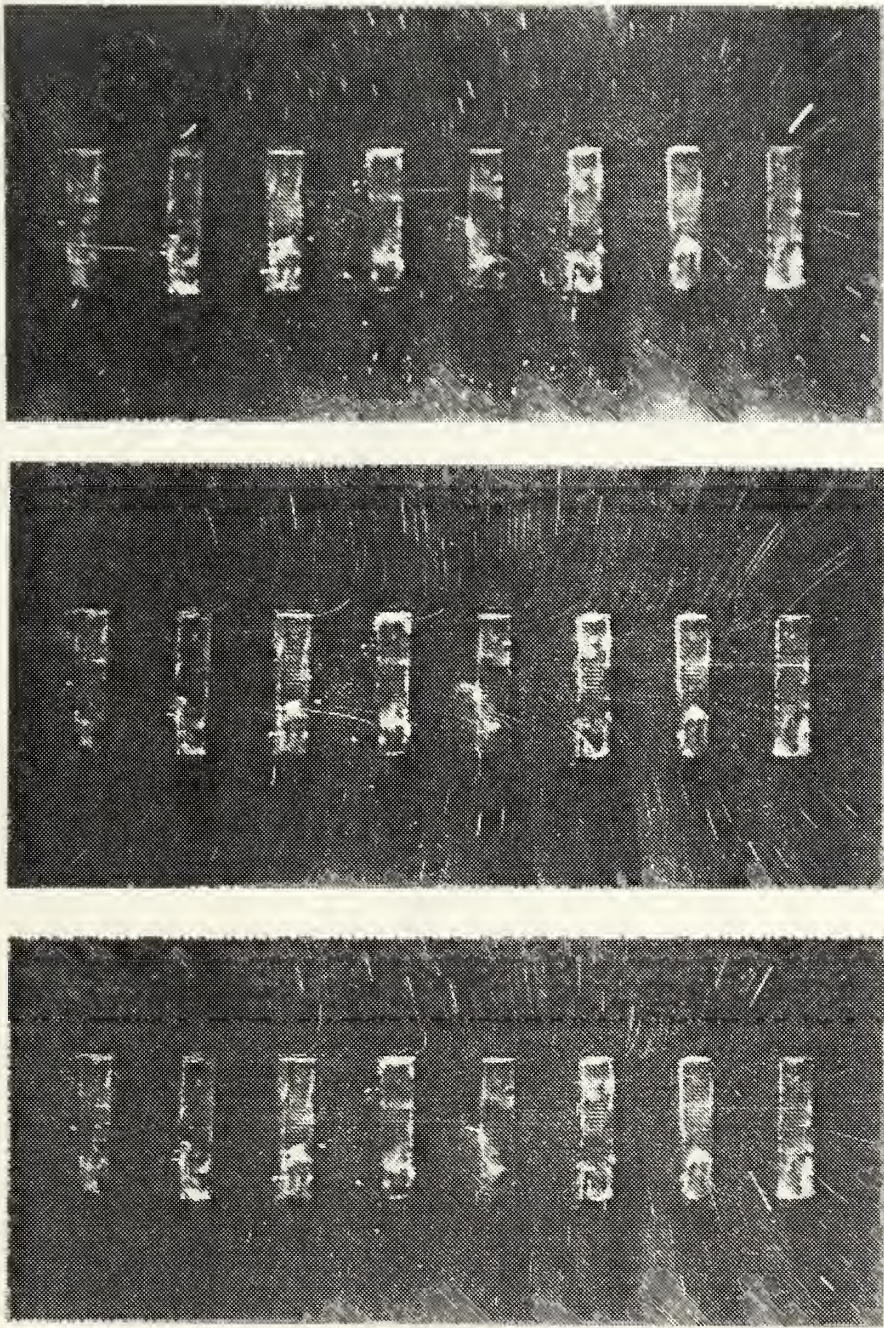
Figure 4.3: Flow in the x-z Plane with 6 mm Shroud Wall

31

figures depict the spread in data on the same plotting scale for the maximum and minimum power levels.

Again it is noted that the general trend, regardless of input power level, is increasing downstream temperature excess. As power is increased from 0.2 watts to 2.0 watts, the values for the non-dimensional temperature excess decrease. As expected, the heat transfer coefficient increases for corresponding components as the power level increases.

There is little difference in the non-dimensional temperature excess as the shroud is positioned 6 mm or more from the substrate. When the shroud is closer to the substrate, it reduces the ambient fluid entrainment, thereby increasing component temperatures. This is less pronounced at the higher power levels as seen in Figure 4.5.

Figure 4.6 shows the actual temperature difference for the component centers versus the shroud position at 2.0 watts. For this case and all other power levels, the actual temperature difference was greater when the shroud was closer than 6 mm from the substrate. When positioned 6 mm or more from the test surface, the actual temperature difference was within $0.5°C$ of the unshrouded levels.

The modified Nusselt numbers for component centers were calculated using the same correlation as in the previous chapter. These values were compared on a logarithmic plot with the flux-based Grashof numbers at each shroud position. The base line curve for the linear least squares fit of the unshrouded data with $\pm5\%$ scatterband was also plotted for comparison. The scatter plot for data when the shroud was positioned 1.5 mm from the substrate is shown in Figure 4.7.

The only points in close agreement with base line data are those points corresponding to the leading heater element. Regardless of power level or shroud position, the leading heater can be treated as a single discrete heat source independent
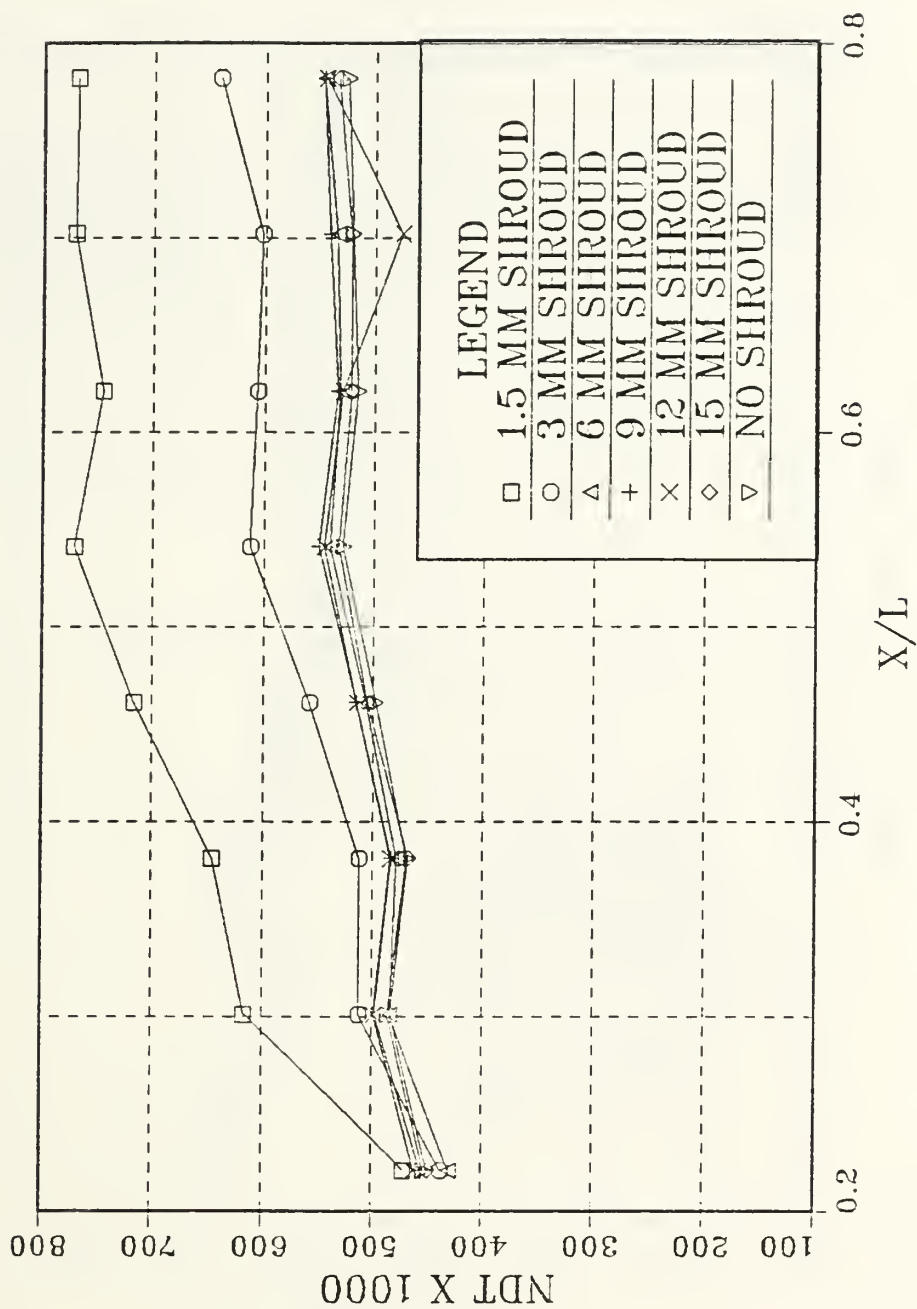
Figure 4.4: Non-dimensional Temperature Excess vs. Position with Shroud at 0.2 Watts

33
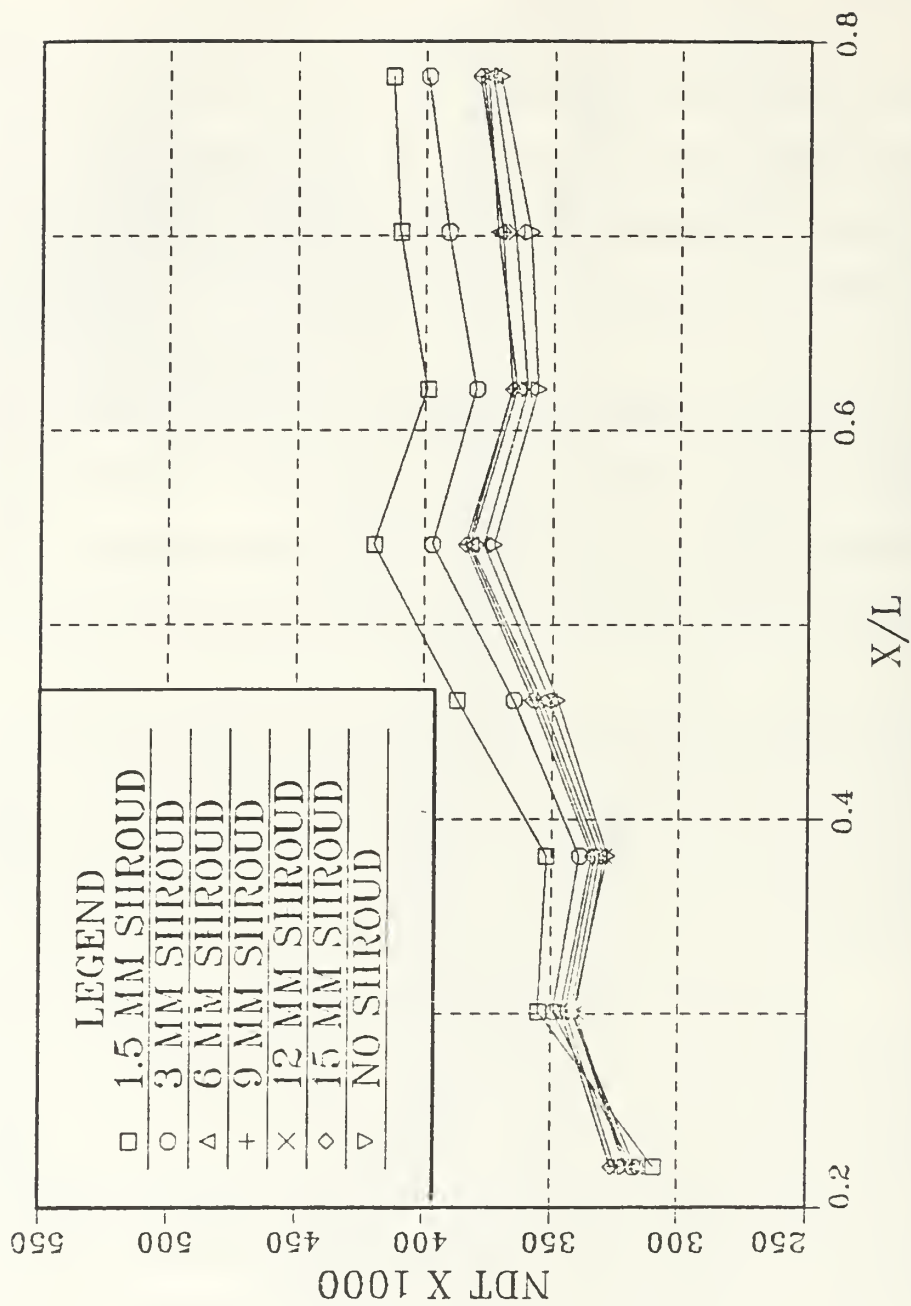
Figure 4.5: Non-dimensional Temperature Excess vs. Position with Shroud at 2.0 Watts

34
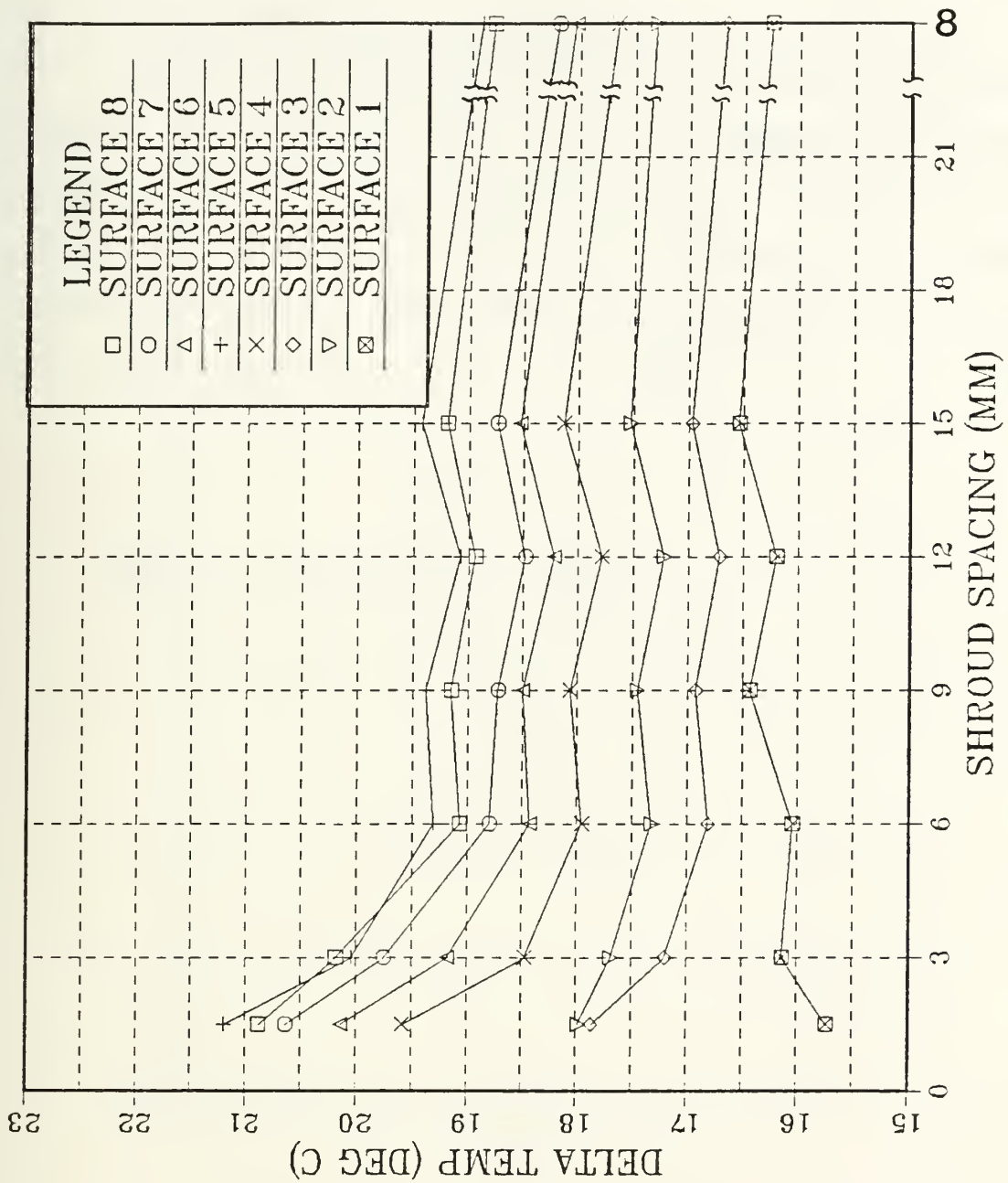
Figure 4.6: Temperature Difference vs. Shroud Spacing: 2.0 Watts

35
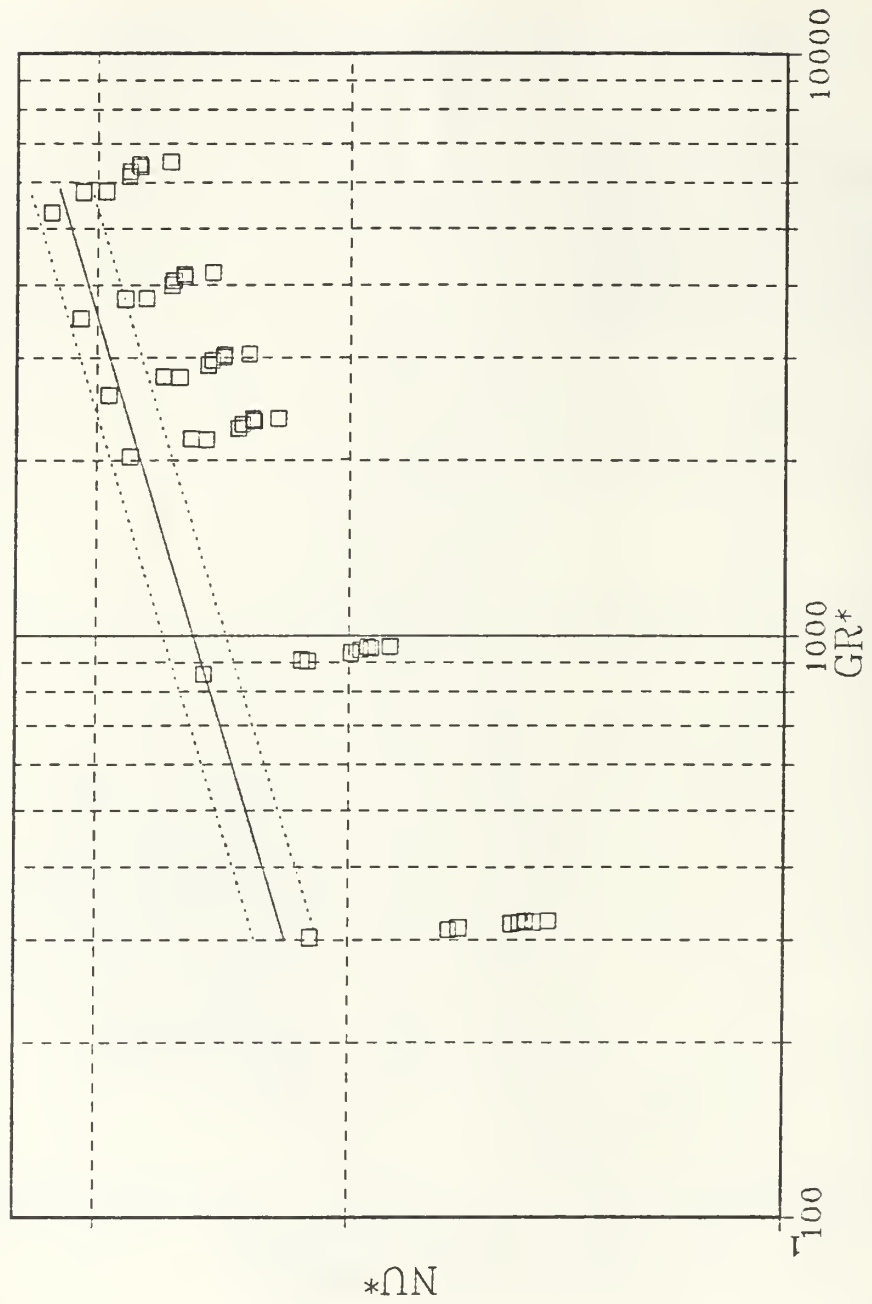
Figure 4.7: Modified Nusselt Number vs. Flux-based Grashof Number with Shroud at 1.5 mm

36

of downstream array geometry. A scatter plot of data for the shroud position of 3.0 mm is not much better than the previous case.

Figure 4.8 shows a plot of modified data when the shroud spacing is increased to 6.0 mm. The same trends seen here were found at all larger spacings. All data are seen to be in close agreement with the correlating equation thus, with a channel width of 6.0 mm or more in width and for the given geometric array, the modified Nusselt number can be calculated to within 5% accuracy using Equation 3.2 for $250 < Gr_x^* < 7000$ and $Pr \sim 7$.

Figure 4.8: Modified Nusselt Number vs. Flux-based Grashof Number with Shroud at 6.0 mm
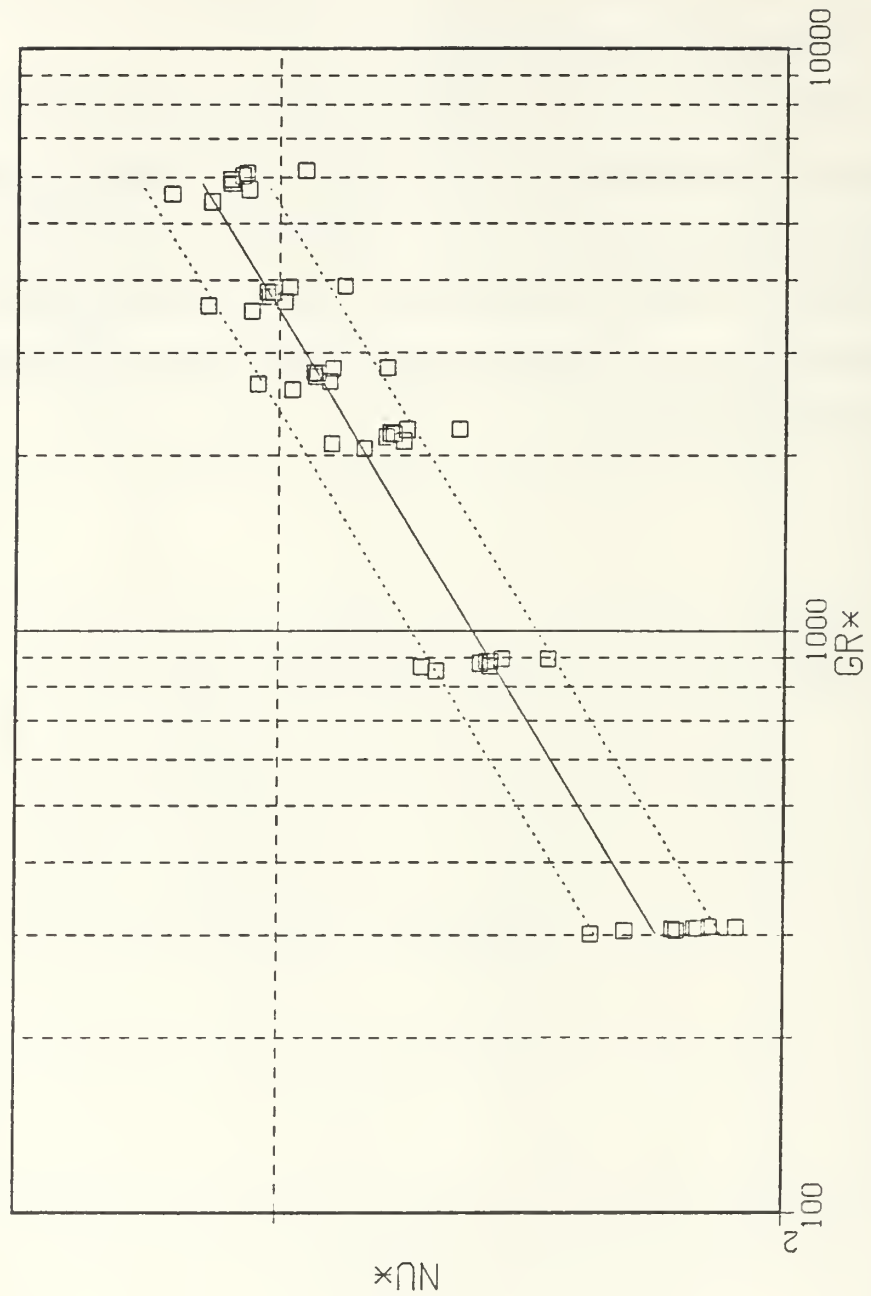
V. CONCLUSIONS

Flow visualization and quantitative analysis provided several significant conclusions:

- The flow was laminar over the given range of power levels.

- The convective flow is nearly two-dimensional when the shroud is not present. This condition greatly simplifies computational modelling of such flows.

- A thermal layer was embedded within the momentum region. This layer became thinner at increasing levels of heat flux.

- A general trend of increasing component temperatures downstream at each power level was found.

- No significant gain in the rate of heat transfer for channel widths of 6.0 mm or more was found over the unshrouded configuration.

- For geometrically similar arrays, heat transfer relationships for downstream components can be determined by using the correlating equation for this geometry.

- As component spacing is increased to two times or more of that for the present configuration, upstream effects become negligible and the heaters can be treated as an individual discrete heat source.

VI. RECOMMENDATIONS

In continuation of this study, it is suggested to use a similar array, however:

- Study the effects of even smaller component spacings on heat transfer.

- Flank each side of the single array with a column of flush mounted heat sources.

- Spray the heater elements with temperature sensitive liquid crystals.

- Measure the variation of temperature within the thermal layer at higher power levels for all components and spaces between components.

- Explore the transient evolution of transport.

APPENDIX A
SOFTWARE

A.   TEMPERATURE ACQUISITION PROGRAM

```
10      !!!!!!!!!!!!!!!!!!!!!!!!!!!!!!!!!!!!!!!!!!!!!!!!!!!!!!!!!!!!!!!!!!!!!!!!!!!
20      !!                    TEMPERATURE ACQUISITION PROGRAM                 !!
30      !!                           (STEADY STATE)                          !!
40      !!!!!!!!!!!!!!!!!!!!!!!!!!!!!!!!!!!!!!!!!!!!!!!!!!!!!!!!!!!!!!!!!!!!!!!!!!!
50      REAL Volts(60)
60      REAL Temp(59)
70      CREATE BDAT "_____:,700,0,_",48
80      ASSIGN @Path3 TO "_____:,700,0,_"
90      PRINT "                        SURFACE #8"
100     PRINT
110     OUTPUT 709;"CONFMEAS DCV,100,USE 0"
120     ENTER 709;Volts(60)
130     OUTPUT 709;"CONFMEAS DCV,100-105,USE 0"
140     FOR I=0 TO 5
150     ENTER 709;Volts(I)
160     Temp(I)=.0006797+(25825.1328*Volts(I))-(607789.2467*(Volts(I)*Volts(I)))-(
21952034.3364*(Volts(I)^3))+(8370810996.1874*(Volts(I)^4))+.075
170     PRINT "T. C.  #";I+1," Volts D.C.  ";Volts(I),"Temp. DEG. C ";Temp(I)
180     NEXT I
190     PRINT
200     PRINT "                        SURFACE #7"
210     PRINT
220     OUTPUT 709;"CONFMEAS DCV,106-111,USE 0"
230     FOR I=6 TO 11
240     ENTER 709;Volts(I)
250     Temp(I)=.0006797+(25825.1328*Volts(I))-(607789.2467*(Volts(I)*Volts(I)))-(
21952034.3364*(Volts(I)^3))+(8370810996.1874*(Volts(I)^4))+.075
260     PRINT "T. C.  #";I+1," Volts D.C.  ";Volts(I),"Temp. DEG. C ";Temp(I)
270     NEXT I
280     PRINT
290     PRINT "                        SURFACE #6"
300     PRINT
310     OUTPUT 709;"CONFMEAS DCV,112-117,USE 0"
320     FOR I=12 TO 17
330     ENTER 709;Volts(I)
340     Temp(I)=.0006797+(25825.1328*Volts(I))-(607789.2467*(Volts(I)*Volts(I)))-(
21952034.3364*(Volts(I)^3))+(8370810996.1874*(Volts(I)^4))+.075
350     PRINT "T. C.  #";I+1," Volts D.C.  ";Volts(I),"Temp. DEG. C ";Temp(I)
360     NEXT I
```

41

```
570    PRINT
580    PRINT                              SURFACE #5
590    PRINT
400    OUTPUT 709;"CONFMEAS DCV,216-219,USE 0"
410    FOR I=16 TO 19
420    ENTER 709;Volts(I)
430    Temp(I)=.0006797+(25825.1325*Volts(I))-(607769.2467*(Volts(I)*Volts(I)))-(
21952034.3364*(Volts(I)^3))+(8370610996.1874*(Volts(I)^4))+.075
440    PRINT "T. C.  #";I+1,"  Volts D.C.  ";Volts(I),"Temp. DEG. C ";Temp(I)
450    NEXT I
460    OUTPUT 709;"CONFMEAS DCV,200-203,USE 0"
470    FOR I=20 TO 23
480    ENTER 709;Volts(I)
490    Temp(I)=.0006797+(25825.1325*Volts(I))-(607769.2467*(Volts(I)*Volts(I)))-(
21952034.3364*(Volts(I)^3))+(8370610996.1874*(Volts(I)^4))+.075
500    PRINT "T. C.  #";I+1,"  Volts D.C.  ";Volts(I),"Temp. DEG. C ";Temp(I)
510    NEXT I
520    PRINT
530    PRINT "                            SURFACE #4"
540    PRINT
550    OUTPUT 709;"CONFMEAS DCV,204-209,USE 0"
560    FOR I=24 TO 29
570    ENTER 709;Volts(I)
580    Temp(I)=.0006797+(25825.1325*Volts(I))-(607769.2467*(Volts(I)*Volts(I)))-(
21952034.3364*(Volts(I)^3))+(8370610996.1874*(Volts(I)^4))+.075
590    PRINT "T. C.  #";I+1,"  Volts D.C.  ";Volts(I),"Temp. DEG. C ";Temp(I)
600    NEXT I
610    PRINT
620    PRINT "                            SURFACE #3"
630    PRINT
640    OUTPUT 709;"CONFMEAS DCV,210-215,USE 0"
650    FOR I=30 TO 35
660    ENTER 709;Volts(I)
670    Temp(I)=.0006797+(25825.1325*Volts(I))-(607769.2467*(Volts(I)*Volts(I)))-(
21952034.3364*(Volts(I)^3))+(8370610996.1874*(Volts(I)^4))+.075
680    PRINT "T. C.  #";I+1,"  Volts D.C.  ";Volts(I),"Temp. DEG. C ";Temp(I)
690    NEXT I
700    FOR J=1 TO 14
710    PRINT
```

42

```
720    NEXT J
730    PRINT "                        SURFACE #2"
740    PRINT
750    OUTPUT 709;"CONFMEAS DCV,216-219,USE 0"
760    FOR I=36 TO 39
770    ENTER 709;Volts(I)
780    Temp(I)=.0006797+(25825.1328*Volts(I))-(607789.2467*(Volts(I)*Volts(I)))-(
21952034.3364*(Volts(I)^3))+(8370810996.1874*(Volts(I)^4))+.075
790    PRINT "T. C.  #";I+1," Volts D.C.  ";Volts(I),"Temp. DEG. C ";Temp(I)
800    NEXT I
810    OUTPUT 709;"CONFMEAS DCV,300-301,USE 0"
820    FOR I=40 TO 41
830    ENTER 709;Volts(I)
840    Temp(I)=.0006797+(25825.1328*Volts(I))-(607789.2467*(Volts(I)*Volts(I)))-(
21952034.3364*(Volts(I)^3))+(8370810996.1874*(Volts(I)^4))+.075
850    PRINT "T. C.  #";I+1," Volts D.C.  ";Volts(I),"Temp. DEG. C ";Temp(I)
860    NEXT I
870    PRINT
880    PRINT "                        SURFACE #1"
890    PRINT
900    OUTPUT 709;"CONFMEAS DCV,302-307,USE 0"
910    FOR I=42 TO 47
920    ENTER 709;Volts(I)
930    Temp(I)=.0006797+(25825.1328*Volts(I))-(607789.2467*(Volts(I)*Volts(I)))-(
21952034.3364*(Volts(I)^3))+(8370810996.1874*(Volts(I)^4))+.075
940    PRINT "T. C.  #";I+1," Volts D.C.  ";Volts(I),"Temp. DEG. C ";Temp(I)
950    NEXT I
960    !OUTPUT @Path3;Temp(*)
970    PRINT
980    PRINT
990    PRINT "                BATH TEMPERATURES (TOP TO BOTTOM)"
1000   PRINT
1010   OUTPUT 709;"CONFMEAS DCV,317-319,USE 0"
1020   FOR I=57 TO 59
1030   ENTER 709;Volts(I)
1040   Temp(I)=.0006797+(25825.1328*Volts(I))-(607789.2467*(Volts(I)*Volts(I)))-(
21952034.3364*(Volts(I)^3))+(8370810996.1874*(Volts(I)^4))+.075
1050   PRINT "VOLTS D.C.  ";Volts(I),"TEMP. DEG. C ";Temp(I)
1060   NEXT I
1070   END
```

B. DATA REDUCTION PROGRAM

```
10      !!!!!!!!!!!!!!!!!!!!!!!!!!!!!!!!!!!!!!!!!!!!!!!!!!!!!!!!!!!!!!!!!!!!!!!
20      !!                                                                !!
30      !!                  DATA REDUCING PROGRAM                         !!
40      !!                                                                !!
50      !!!!!!!!!!!!!!!!!!!!!!!!!!!!!!!!!!!!!!!!!!!!!!!!!!!!!!!!!!!!!!!!!!!!!!!
60      REAL T(43),Qcond(8)
70      REAL Power,Tamb,G,Kpg,Delx,As,Per,Ta,Qconv,Lbar
80      REAL Qflux,Delt,Tfilm,Beta,Spvol,Dynvisc
90      REAL Kinvisc,Kf,Pr,Theta,Ndt,Hx,Grmod,Hux,Lnu,Lgr
100     PRINTER IS 1
110     PRINT "INPUT DATA FILE NAME"
120     INPUT Filename$
130     PRINT
140     PRINT "INPUT POWER VALUE IN WATTS"
150     INPUT Power
160     PRINT
170     PRINT "INPUT SHROUD SPACING IN mm"
180     INPUT Space$
190     PRINT
200     PRINT "INPUT AMBIENT TEMPERATURE"
210     INPUT Tamb
220     PRINTER IS 701
230     PRINT "POWER LEVEL (WATTS)      :",Power
240     PRINT
250     PRINT "SHROUD POSITION (mm)     :",Space$
260     PRINT
270     PRINT "AMBIENT TEMPERATURE (C)  :",Tamb
280     PRINT
290     PRINT
300     ASSIGN @Path TO Filename$
310     ENTER @Path;T(*)
320     G=9.81
330     Kpg=.1421
340     Delx=.006731
350     As=.0239*.0078
360     Per=2*.0239+2*.0078
370     Lbar=As/Per
380     A$="Qcond"
```

44

```
390    B$="X/L"
400    C$="NDT"
410    D$="LOG(Nu.)"
420    E$="LOG(Grx*)"
430    F$="DELT"
440    G$="H."
450    H$="Nux"
460    I$="Grx*"
470    !!!!!!!!!!!!!!!!!!!!!!!!!!!!!!!!!!!!!!!!!!!!!!!!!!!!!!
480    !          COMPUTE CONDUCTION LOSSES          !
490    !!!!!!!!!!!!!!!!!!!!!!!!!!!!!!!!!!!!!!!!!!!!!!!!!!!!!!
500    J=8
510    FOR I=0 TO 42 STEP 6
520    Ta=(T(I)+T(I+1)+T(I+2)+T(I+3)+T(I+4))/5
530    Qcond(J)=As*Kpg*(Ta-T(I-5))/Del*
540    J=J-1
550    NEXT I
560    !!!!!!!!!!!!!!!!!!!!!!!!!!!!!!!!!!!!!!!!!!!!!!!!!!!!!!
570    N=0
580    FOR J=8 TO 1 STEP -1
590    Cnt=0
600    Xt=((J-1)*25.4+74)/317
610    Xb=((J-1)*25.4+66)/317
620    Xc=((J-1)*25.4+70)/317
630    PRINT
640    PRINT
650    PRINT "                              SURFACE #",J
660    PRINT
670    PRINT USING "2X,AAAAA,4X,AAA,4X,AAA,4X,AAAAAAAA,2X,AAAAAAAAA,3X,AAAA,5X,AA
,6X,AAA,4X,AAAA";A$,B$,C$,D$,E$,F$,G$,H$,I$
680    FOR I=N TO N+4
690    Qconv=Power-Qcond(J)
700    Qflux=Qconv/As
710    Delt=T(I)-Tamb
720    Tfilm=273.15+(T(I)+Tamb)/2
730    Beta=(-7.944858E-8*(Tfilm^2))+(5.7356479E-5*Tfilm)-.0097810563
740    Spvol=(4.69699E-9*(Tfilm^2))+(-2.53745E-6*Tfilm)+.001341903
750    Dynvisc=(3.2348511E-7*(Tfilm^2))+(-.00021474487*Tfilm)+.036166792
760    Kinvisc=Spvol*Dynvisc
```

```
770    Kf=(1.418181818E-3*Tfilm)+.1866
780    Pr=(4.65706E-3*(Tfilm^2))+(-2.922094*Tfilm)+463.3319
790    Theta=Qflux*Lbar/Kf
800    Ndt=Delt/Theta
810    Hx=Qflux/Delt
820    Grmod=(G*Beta*Qflux*(Lbar)^4)/(Kf*Kinvisc^2)
830    Nux=Hx*Lbar/Kf
840    Lgr=LGT(Grmod)
850    Lnu=LGT(Nux)
860    IF Cnt=0 THEN Xtol=Xt
870    IF Cnt=1 THEN Xtol=Xb
880    IF Cnt>1 THEN Xtol=Xc
890    Cnt=Cnt+1
900    PRINT USING "1X,D.DDDD,2X,D.DDD,2X,D.DDD,4X,D.DDD,7X,D.DDD,4X,DD.DDD,2X,DD
DD.D,2X,DD.DDD,2X,DDDD.D";Qccnd(J),Xtol,Ndt,Lnu,Lgr,Delt,Hx,Nux,Grmod
910    NEXT I
920    N=N+6
930    NEXT J
940    END
```

APPENDIX B
EQUATIONS

A. SAMPLE CALCULATIONS

These calculations are based on temperatures from data corresponding to surface eight with all elements powered to 1.0 Watt and no shroud.

1. CHARACTERISTIC DIMENSIONS

$$P = 2(0.0078 + 0.0239)$$

$$= 0.063m \tag{B.1}$$

$$A_s = (0.0078)(0.0239)$$

$$= 1.864 \times 10^{-4} m^2 \tag{B.2}$$

$$\bar{L} = \frac{1.864 \times 10^{-4}}{0.0634}$$

$$= 2.940 \times 10^{-3} m \tag{B.3}$$

2. CONDUCTION LOSS

$$T_{avg} = \frac{30.40 + 27.98 + 27.09 + 27.39 + 31.11}{5}$$

$$= 28.79°C \tag{B.4}$$

$$Q_{COND} = \frac{(1.864 \times 10^{-4})(0.1421)(28.79 - 26.09)}{.006731}$$

$$= 0.0106W \tag{B.5}$$

3. CONVECTED HEAT FLUX

$$Q_{CONV} = 1.0 - 0.0106$$

47

$$= \quad 0.9894W \tag{B.6}$$

$$q'' \quad = \quad \frac{0.9894}{1.864 \times 10^{-4}}$$

$$= \quad 5308 \frac{W}{m^2} \tag{B.7}$$

4. FLUID PROPERTIES

$$T_{film} \quad = \quad \frac{31.11 + 20.55}{2} + 273.15$$

$$= \quad 298.98K \tag{B.8}$$

$$\beta \quad = \quad (-7.945 \times 10^{-8})(298.98) + (5.736 \times 10^{-5})$$

$$(298.98) - 9.781 \times 10^{-3}$$

$$= \quad 2.665 \times 10^{-4} K^{-1} \tag{B.9}$$

$$v \quad = \quad (4.697 \times 10^{-9})(298.98)^2 - (2.537 \times 10^{-6})(298.98)$$

$$+1.342 \times 10^{-3}$$

$$= \quad 1.003 \times 10^{-3} \frac{m^3}{kg} \tag{B.10}$$

$$\mu \quad = \quad (3.235 \times 10^{-7})(298.98)^2 - (2.147 \times 10^{-4})(298.98)$$

$$+0.0362$$

$$= \quad 9.264 \times 10^{-4} \frac{Ns}{m^2} \tag{B.11}$$

$$\nu \quad = \quad (1.003 \times 10^{-3})(9.264 \times 10^{-4})$$

$$= \quad 9.262 \times 10^{-7} \frac{m^2}{s} \tag{B.12}$$

$$k_f \quad = \quad (1.418 \times 10^{-3})(298.98) + 0.1866$$

$$= \quad 0.611 \frac{W}{mK} \tag{B.13}$$

5. NON-DIMENSIONAL TEMPERATURE EXCESS

$$\theta \quad = \quad 31.11 - 20.55 = 10.56°C \tag{B.14}$$

48

$$\theta_o \quad = \quad \frac{(5308)(2.940 \times 10^{-3})}{0.611} = 25.54°C \qquad (B.15)$$

$$NDT \quad = \quad \frac{10.56}{25.54} = 0.413 \qquad (B.16)$$

6. HEAT TRANSFER COEFFICIENT

$$h_x = \frac{5308}{31.11 - 20.55} = 502.7 \frac{W}{m^2 K} \qquad (B.17)$$

7. FLUX-BASED GRASHOF NUMBER

$$Gr_x^* = \frac{(9.81)(2.665 \times 10^{-4})(5308)(2.940 \times 10^{-3})^4}{(0.611)(9.292 \times 10^{-7})^2} = 1965 \qquad (B.18)$$

8. NUSSELT NUMBER

$$Nu = \frac{(502.7)(2.940 \times 10^{-3})}{0.611} = 2.419 \qquad (B.19)$$

LIST OF REFERENCES

1. Hannemann, R., Incropera, F. P., and Simons, R., "Single Phase Liquid Cooling," *Research Needs in Electronic Cooling*, pp. 6-25, December 1986.

2. Milanez, L. F. and Bergles, A. E., "Studies on Natural Convection Heat Transfer from Thermal Sources on a Vertical Surface," *Proceedings of the Eighth International Heat Transfer Conference*, Vol. 3, pp. 1347-1352, 1986.

3. Johnson, C. B., "Evaluation of Correlations for Natural Convection Cooling of Electronic Equipment," *Heat Transfer Engineering*, Vol. 7, pp. 36-45, 1986.

4. Park, K. A. and Bergles, A. E., "Natural Convection Heat Transfer Characteristics of Simulated Microelectronic Chips," *Journal of Heat Transfer - 1987*, ASME, HTD-Vol. 109, pp.90-96.

5. Hazard, S. J., "Single Phase Liquid Immersion Cooling of Discrete Heat Sources in a Vertical Channel," M.S.M.E. Thesis, Naval Postgraduate School, Monterey,CA , December 1987.

6. Baker, E., "Liquid Cooling of Microelectronic Devices by Free and Forced Convection," *Microelectronics and Reliability*, Pergamon Press, Vol. 11, pp. 213-222, 1972.

7. Willson, T. D., "A Study of Natural Convection Cooling of Multiple Discrete Heat Sources in a Vertical Channel," M.S.M.E. Thesis, Naval Postgraduate School, Monterey, CA , June 1988.

8. Incropera, F. P., and DeWitt, D. P., *Fundamentals of Heat and Mass Transfer*, p. 774, John Wiley and Sons, 1981.

INITIAL DISTRIBUTION LIST

No. of Copies

1. Defense Technical Information Center 2
   Cameron Station
   Alexandria, VA 22304-6145

2. Library, Code 0142 2
   Naval Postgraduate School
   Monterey, CA 93943-5002

3. Mr. Howard Stevens 1
   Head, Electrical Research Center
   David Taylor Research Center
   Annapolis, MD 21402

4. Superintendent 1
   Naval Postgraduate School
   Attn: Professor A. J. Healey, Code 69Hy
   Department of Mechanical Engineering
   Monterey, CA 93943-5004

5. Superintendent 3
   Naval Postgraduate School
   Attn: Professor Y. Joshi, Code 69Ji
   Department of Mechanical Engineering
   Monterey, CA 93943-5004

6. Superintendent 1
   Naval Postgraduate School
   Attn: Professor M. D. Kelleher, Code 69Kk
   Department of Mechanical Engineering
   Monterey, CA 93943-5004

7. Superintendent 1
   Naval Postgraduate School
   Attn: Professor A. D. Kraus, Code 62Ks
   Department of Electrical and Computer Engineering
   Monterey, CA 93943-5004

8. Mr. Duane Embree   1
    Naval Weapons Support Center
    Code 0642
    Crane, IN 47522

9. Superintendent   1
    Naval Postgraduate School
    Attn: Curricular Officer, Code 34
    Monterey, CA 93943-5004

10. Superintendent   1
    Naval Postgraduate School
    Attn: Lt. Al Gaiser
    SMC 2007
    Monterey, CA 93943-5000

11. Mr. Joseph Cipriano   1
    Executive Director
    Weapons and Combat Systems Directorate
    Naval Sea Systems Command
    Washington, D.C. 20362-5101

12. Lt. Daniel L. Knight   1
    Rt. 1, Box 224A
    Warrenville, S.C. 29851